Underwater navigation based on passive electric sense: New perspectives for underwater docking

Frédéric Boyer, Vincent Lebastard, Christine Chevallereau, Stefano Mintchev, Cesare Stefanini

▶ **To cite this version:**

Frédéric Boyer, Vincent Lebastard, Christine Chevallereau, Stefano Mintchev, Cesare Stefanini. Underwater navigation based on passive electric sense: New perspectives for underwater docking. The International Journal of Robotics Research, 2015, 34 (9), pp.1228-1250. 10.1177/0278364915572071 . hal-01201695

HAL Id: hal-01201695
https://imt-atlantique.hal.science/hal-01201695

Submitted on 11 Apr 2017

HAL is a multi-disciplinary open access archive for the deposit and dissemination of scientific research documents, whether they are published or not. The documents may come from teaching and research institutions in France or abroad, or from public or private research centers.

L'archive ouverte pluridisciplinaire **HAL**, est destinée au dépôt et à la diffusion de documents scientifiques de niveau recherche, publiés ou non, émanant des établissements d'enseignement et de recherche français ou étrangers, des laboratoires publics ou privés.

Underwater navigation based on passive electric sense: new perspectives for underwater docking

Frederic Boyer[1], Vincent Lebastard[1], Christine Chevallereau[1],
Stefano Mintchev[2] and Cesare Stefanini[2]

December 22, 2014

Abstract

In underwater robotics, several homing and docking techniques are currently being investigated. They aim to facilitate the **recovery** of underwater vehicles, as well as their connection to underwater stations for battery charging and data exchange. **Developing reliable underwater docking strategies is a critical issue** especially in murky water or/and in confined and cluttered environments. Commonly used underwater sensors such as sonar and camera can fail in these conditions. We show how a bio-inspired sensor could be used to help guide an underwater robot during a docking phase. The sensor is inspired by the passive electro-location ability of electric fish. Exploiting the electric interactions and the morphology of the vehicle, a sensor based reactive control law is proposed. **It allows the guidance of the robot** toward the docking station by following an exogenous electric field generated by a set of electrodes fixed to the environment **This is achieved while avoiding insulating perturbative objects**. This control strategy is theoretically analysed and validated with experiments carried out on a setup dedicated to the study of electric sense. **Though promising, these results are but a first step towards the implementation of an approach to docking in more realistic conditions, such as in turbid salt water or in the presence of conductive perturbative objects.**

Keywords: Underwater navigation, electric sense, bio-inspiration, docking strategy.

1 Introduction

Underwater robotic applications such as the examination of marine wreckage, or the exploration of caves, underground rivers, ocean monitoring, maintenance of offshore structures or following catastrophes as those of Fukushima (Japan) or sinking of the Costa Concordia boat (Italy), are vital topics for academia, industry and society.

Remotely Operated Vehicles (ROVs) are currently the most commonly available underwater robots. They are remotely controlled by an operator through a cable connected to a mother vessel, and their use is limited due to high operational costs and operator fatigue [Yuh et al., 2011]. To overcome these limitations, recent research efforts have focused on the development of Autonomous Underwater Vehicles (AUVs). Its self-contained design and decision-making capabilities, allow an **AUV to operate without direct supervision, freed from a tethering cable**. However,

most AUVs need to surface periodically in order to update mission parameters, upload collected data, and recharge their batteries. Data and energy storage capabilities are the main constraints on the duration of an AUV mission.

Underwater homing/docking techniques are a promising solution to the extension of the autonomy of AUVs. Instead of **periodically suspending** its mission in order to surface, an AUV could dock with a submerged station, exchange data and energy, and then continue its tasks. A successful docking approach **depends upon** reliable and robust guidance and navigation algorithms, as well as precise sensors. Underwater docking based on different sensing technologies and control strategies has been the object of considerable work over the last two decades [Krupinski et al., 2008]. State of the art techniques exploit vision based servoing [Lee et al., 2002, Park et al., 2009b, Park et al., 2009a], sonar guidance [Hobson et al., 2007], a mix of sonar and vision, [Brignone et al., 2007, Maki et al., 2013, Kondo et al., 2012] or magnetic field sensing [Feezor et al., 2001]. Nevertheless, underwater docking is still challenging in confined or unstructured environments and in turbid water. The difficulties arise because commonly used underwater sensors are inadequate in these conditions. **Turbidity blocks visual sensors while clutter leads to severe multipath issues which can affect the reliability of sonar [Knight et al., 1981].**

Pursuing a bioinspired approach, a solution based on electric field sensing or more simply "electric sense" could be implemented to address this challenge. Electric sense is a mode of perception evolved **by several hundred fresh water fish species, named active electric fish** [Moller, 1995], as well as sharks and rays [Kalmijn, 1966]. **To perceive their surroundings, active electric fish generate a dipolar electric field by polarizing a specific Electric Organ (EO) located just anterior to the tail with respect to the rest of their body.** Perturbations in the electric field caused by the surroundings (i.e. objects or other fish) are then measured by dedicated receptor organs, which are distributed over their skin. By processing this "electric image", the fish perceive their surroundings and can navigate efficiently in cluttered environments and murky waters with an omnidirectional sensing range of about one body length [Emde et al., 1998]. In contrast to the active electric fish, sharks and rays use only passive electric sense to find their prey following the electric fields generated by the muscular activity of any animal [Bullock and Heiligenberg, 1986, Moller, 1995], and can navigate along the telluric electric fields which pre-exist in their environment. Active electric fish have also evolved a passive version of the electric sense and can perceive the electric field generated by an exogenous electric source such as a conspecific fish [Hopkins, 2009].

This has been studied through biological experiments [Davis and Hopkins, 1988, Hopkins, 2009] in which a living fish and an artificial electric dipole (2 electrodes of opposite charge close to each other) were placed in a same tank (see Figure 1). At a given instant, a voltage was applied between the electrodes that mimicked the field of a conspecific intruder. Obeying a territorial behavior, the fish attacked its artificial rival, seeking it by climbing up the electric lines which emanate from the emitter of the electric dipole (see Figure 1). An implementation based on this strategy seems a promising solution to the problem of underwater docking in confined environments and murky waters. The idea would be to equip a docking station with electrodes generating an electric field, which can be used to guide the robot toward the docking point. This article is a theoretical and experimental analysis of this strategy.

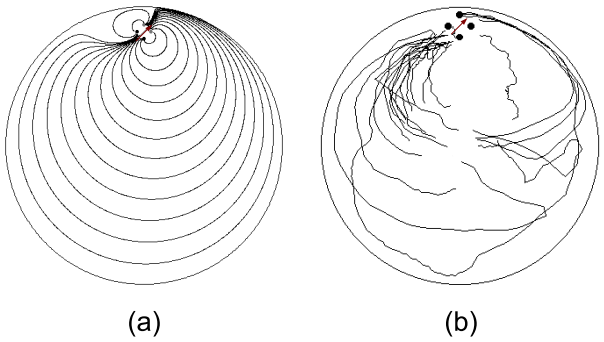

Figure 1: After Hopkins **(a)** Electric lines emanating and returning to an active dipole submerged in a tank with circular insulating boundaries. **(b)** Several fish trajectories recorded by a camera. At each of the trials, the fish seeks the active dipole by following its electric lines.

In principle, any sensor bio-inspired from electric fish is composed of an arbitrary number of electrodes fixed to an insulating shell of a probe or an underwater robot [Silverman et al., 2012, Mintchev et al., 2012] (see Figure 2). A voltage generator imposes a given voltage U on one of the electrodes - the emitter - while the other electrodes - the receivers - are set to ground. When immersed in a conductive fluid, such a sensor generates a dipolar electric field in its surroundings. Any nearby object will perturb the electric field generated by the sensor. Exploiting this basic idea, **MacIver** and his co authors developed a sensor able to measure the voltage perturbation of a set of pairs of floating ground electrodes [MacIver and Solberg, 2001, MacIver et al., 2004, Silverman et al., 2012] symmetrically arranged between one emitter and one receiver. Our approach has been to propose an alternative technological solution, measuring the perturbations in the electric field through the electric currents flowing across a set of receivers set under voltage with respect to the emitter [Servagent et al., 2013]. Based on this principle, several contributions have been recently addressed for electric sensing in underwater-robotics. In [Boyer et al., 2012] a concise analytic model for electrolocation has been proposed and integrated in a Kalman filter in [Baffet et al., 2008, Lebastard et al., 2010], where the problem of reconstruction of the environment and navigation in a tank containing simple shaped objects was addressed. The collective navigation of a group of electric robots has been also addressed for a swarm of rigid vehicles [Chevallereau et al., 2012] or for a swarm of swimming robots [Morel et al., 2012]. More recently, a free-model based navigation approach in encumbered environments [Lebastard et al., 2012, Boyer and Lebastard, 2012] has been proposed. The approach is based on the exploitation of the morphology of the sensors (slender shape, bi-lateral symmetry) and the direct feedback of the measurements of the electric field perturbations. As explained in [Lebastard et al., 2012], it consists of reactions to the electric lines emitted by the polarized objects, in order to seek or to avoid the objects depending on their conductivity with respect to water. In this article, a similar strategy is developed but in the passive case. **The robot follows the field lines of an exogenous ambient electric field generated by a set of external electrodes (one emitter and several receivers) in order to seek the emitter located on the docking station. This is achieved while avoiding the insulating objects along the path to the emitter. The case of perturbative conductive objects is also addressed as a future perspective of this work.** This strategy is complementary to available docking techniques allowing an AUV to be guided toward a submerged docking station in murky waters in a highly complex and cluttered environments.

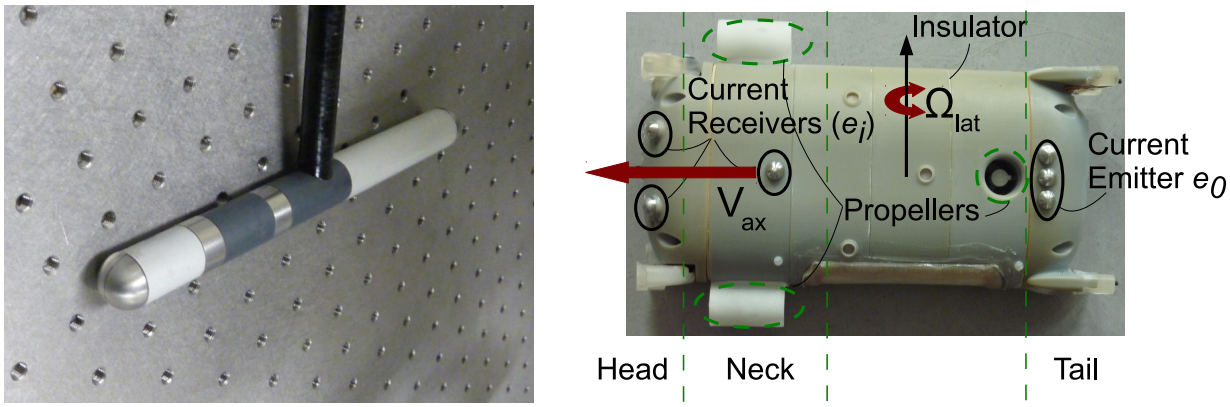

(a) (b)

Figure 2: **Two examples of artificial electric sense robotics systems** (a) Picture of a 7-electrode probe organized in 4 polarizable rings, 3 of them (the receivers) being divided in two half rings obeying a bilateral (left/right) symmetry. **The probe is attached to a vertical rod moved by a controlled gantry.** (b) **ANGELS: the first autonomous underwater robot capable of navigating with electric sense** [Mintchev et al., 2012]. It is driven by three propulsion units (encircled with dashed lines) which allow the robot to be steered and moved forwards and backwards. The robot has an insulating shell on which is fixed a set of hemispherical electrodes disposed in a bilateral symmetric arrangement.

The article is structured as follows. First we will briefly present the sensor technology and the test-bed (section 2) on which the experiments were carried out. Then, we present the models of locomotion and perception in section 3. These models are validated in section 3.2. In section 5, a solution to our starting navigation problem is proposed. The solution is implemented on the experimental test-bed in section 6. The article concludes with **a discussion and perspectives for future research in section 7**.

2 The electrolocation test-bed

2.1 The sensor principle

We have built a set of sensors to study electrolocation [Servagent et al., 2013]. Because of their low aspect ratio (thickness/length) morphology, these sensors are named "slender probes." A schematic view of the most simple probe, the 3-electrode probe, is shown in Figure 3. It consists of an insulating cylindric shell that is 20 cm long with a conductive metallic hemisphere at each end. It is 2cm in diameter. One of these hemispheres is designated the tail e_0, the other forms the head. This head-electrode is divided into a pair of two identical left-right electrodes e_1 and e_2. In active electrolocation [Boyer et al., 2012], the tail-electrode e_0 has a controlled voltage U imposed with respect to (e_1, e_2), which define the common ground of the electric sensor (see Figure 3). When it is immersed in a conductive fluid, this active device produces a field of current lines flowing through the surrounding fluid from the emitting electrode e_0 to the grounding receivers e_1 and e_2 (Figure 3a). The currents flowing across e_1 and e_2 are measured using an electronic measurements board, and aggregated into a vector of measured currents $\mathbf{I} = (I_1, I_2)^T$. The conservation of currents is imposed to the emitter current to satisfy $I_0 = -(I_1 + I_2)$ and is not measured. When there is no

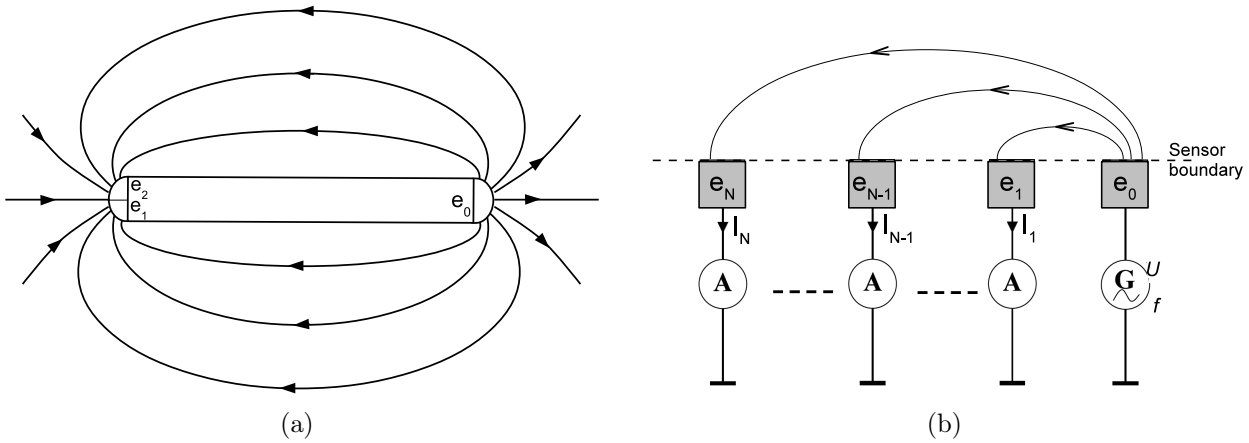

(a) (b)

Figure 3: (a) Illustration of the dipolar electric field generated in active mode by a 3-electrode probe. (b) Principle of the $U-I$ measurement mode for an active probe with an arbitrary number of receptor electrodes.

object near the sensor, the controlled voltage and the measured currents are related through the following model:

$$\mathbf{I} = C^{(0)}U, \tag{1}$$

where $C^{(0)}$ is a (2×1) conductivity matrix of the sensor with no object nearby. It depends on the geometry of the sensor and on the conductivity of the ambient fluid . This matrix can be easily measured in a preliminary calibration phase [Servagent et al., 2013]. When the generator G of the sensor is not active, all of the electrodes are grounded and the sensor is said to be in passive mode. When it is immersed in a fluid through which an imposed external electric field is flowing, the current lines penetrate the electrodes of the passive sensors while still satisfying the current conservation law (Figure 4(a)). The currents flowing across the two head electrodes are measured with the same electronic measurement board as in the active mode and aggregated as the measurement vector $\mathbf{I} = (I_1, I_2)^T$. **The standard electronic measurement board is described in [Servagent et al., 2013]. The detection threshold of this sensor is** $\pm 1e-7$ **A in both active and passive mode, yielding a sensitivity of about** $\pm 0.1\%$ **in active mode in ordinary tap water of conductivity** 400μ**S/m. With an imposed voltage** $U = 5$**V, the sensor range is about one sensor length [Servagent et al., 2013] and comparable to that of an active electric fish. The sensitivity is similar** ($\pm 0.1\%$) **for passive electric sensing in tap water, yielding a range about 3 times the probe length with an externally imposed voltage** $U_e = 10$**V.**

2.2 Tank and cartesian robot

We have built an automated test bench to evaluate our sensors and algorithms (see Figure 5). Our test bench is composed of a cubic tank of one meter side with insulating walls and a three-axis cartesian robot mounted on a gantry above. The tank is filled with ordinary tap water whose conductivity varies from 350 to 420μS/cm. The gantry allows controlled translations of the probe along the horizontal x and y axes (0.3m/s). The θ-orientation in the (x, y) plane can be controlled with a yaw-rotation stage capable of rotation speeds of 13.5rpm. The height of the sensor in the tank is determined by the length of a rigid glass epoxy fibre tube on which it is mounted.

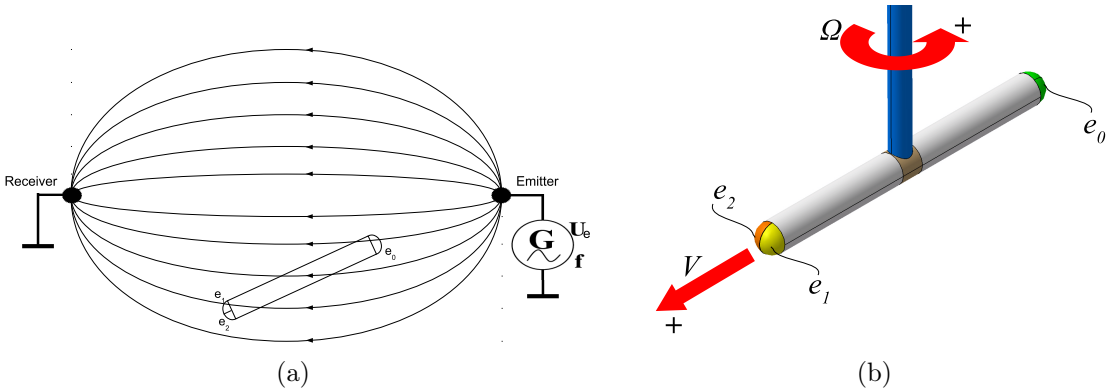

Figure 4: (a) Illustration of the dipolar electric field generated by external electrodes and measured by a 3-electrode probe. (b) Schematic view of a 3-electrode sensor organized in 2 polarizable rings, one of them (located in the head) being divided in two half rings allowing two lateral current measurements.

This vertical tube houses the connecting wires that transmit the signal from the electrodes to the board. At the board the signal is amplified and filtered trough analogue chain then digitalized using a 16 bit ADC Dspace card ($DS2004$). The Dspace card ($DS2004$) converts up to 16 channels simultaneously with a resolution of 0.3mV/bit (LSB) and a maximum conversion speed of 1.25 MHz. Our test bench is described in more detail in [Servagent et al., 2013].

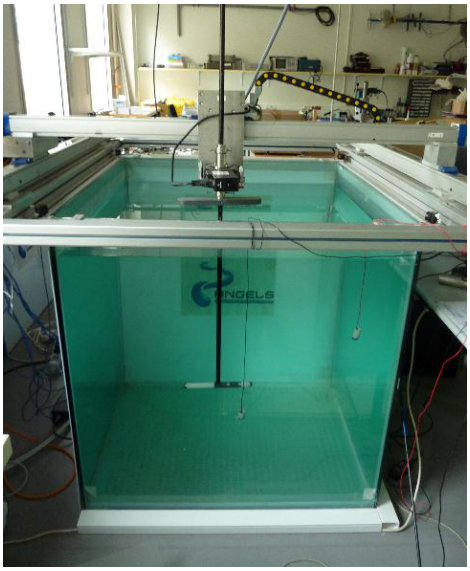

Figure 5: Electric test bench: **A cubical tank 1 meter side above which is an actuated gantry enables control of the motion of the probes see Figure 2.a.**

3 Model of locomotion and passive electro-location

In this section, we derive a model for the control of a passive probe. This includes a model of locomotion (section 3.1) and a model of electric perception (section 3.2).

3.1 Model of locomotion

In the following, the study will be focused on a sensor moving in a static environment. Due to the constraints imposed by the gantry (section 2.2), the sensor moves in a horizontal equatorial plane of the sensor. The objects were placed in this equatorial plane of the sensor **to enable them to be best perceived**. The movements imposed on the sensor are those of a non-holonomic unicycle able to move along the sensor length and to rotate around the vertical stick. This restriction of the sensor's motion corresponds to the planar motion of most AUVs or that of a swimming fish which cannot move laterally while stabilizing its roll velocity to zero. The sensor moves with an axial linear velocity V aligned along the sensor axis and oriented positively toward the head. The yaw angular velocity Ω is orthogonal to the plane of the scene (see Figure 4(b)). With this assumption, the locomotion model can be reduced to the kinematic model:

$$\begin{pmatrix} \dot{x} \\ \dot{y} \\ \dot{\theta} \end{pmatrix} = \begin{pmatrix} \cos\theta & \frac{l\sin\theta}{2} \\ -\sin\theta & \frac{l\cos\theta}{2} \\ 0 & 1 \end{pmatrix} \begin{pmatrix} V \\ \Omega \end{pmatrix}, \tag{2}$$

where, $(x, y, \theta)^T$ is the vector of Cartesian pose of a frame attached to the sensor head related to a fixed frame $(O, \mathbf{e}_x, \mathbf{e}_y)$ attached to the plane of the scene. Finally, in the following, (V, Ω) define the control inputs of the sensor whose motions are modeled through (2).

3.2 Electric model of a passive sensor in an ambient field with small objects

In this subsection, we address the problem of modelling a passive sensor in the presence of small objects immersed in an exogenous electric field produced by a set of punctual external electrodes, one being an emitter, the others being receivers. The receivers are all grounded while the emitter is set to a given voltage U_e.

3.2.1 Statement of the problem

Being in the regime of the quasi-static approximation of electromagnetism [Jackson, 1962], the electric state of the scene surrounding the passive sensor can be completely parameterized by an electric potential ϕ solution at each time of the Laplace equations:

$$\Delta\phi = 0, \tag{3}$$

with boundaries conditions imposed on the sensor and the objects in the scene. To derive the model of currents measured by the passive sensor, one needs the constitutive Ohm's law:

$$\mathbf{j} = -\gamma_0 \boldsymbol{\nabla}\phi, \tag{4}$$

which relates the currents flowing in the water $\mathbf{j}$ to the electric field $-\boldsymbol{\nabla}\phi$, with γ_0 the water conductivity, which is assumed to be electrically homogeneous and isotropic. Each measured current I_k is defined as the flux of the current field flowing across the e_k electrode. Thus, the vector of measurements can be detailed as:

$$\mathbf{I} = (I_1, I_2)^T = \gamma_0 (\int_{e_1} \boldsymbol{\nabla}\phi.\mathbf{n}ds, \int_{e_2} \boldsymbol{\nabla}\phi.\mathbf{n}ds)^T, \tag{5}$$

where $\mathbf{n}$ is the inward normal to the sensor boundaries. In [Boyer et al., 2012], the analytical resolution of (3-5) has been addressed through the method of reflections [Happel and Brenner, 1965] for scenes constituted by an active sensor in the presence of one and several small objects. Using this approach, it is possible to show that the electric currents flowing across the passive sensor electrodes represent the electric reaction of the passive sensor when it has a voltage imposed by a potential field of the form:

$$\phi_a = \phi^{(0)} + \phi^{(1)}, \tag{6}$$

where $\phi^{(0)}$ and $\phi^{(1)}$ **(the upper index denotes the successive reflections travelling in the scene)** respectively denote the external exogenous field produced by the external electrodes, and the potential field emitted by the objects polarized by $\phi^{(0)}$. Physically, ϕ_a **pushes the sensor out of** its electric balance, while the currents which flow across the electrodes make it to recover its equilibrium (this is the electric reaction of the sensor to the applied field). In the following, we are going to model the electric measurements of the passive sensor when it is immersed with small objects in an ambient field generated by external electrodes. To that end, we will proceed in two steps. First, we will derive the model of the response of the passive sensor when it is introduced into any ambient field ϕ_a (section 3.2.2). Secondly, in section 3.2.3 we will present the model of ϕ_a in the case where it is generated by external electrodes in the presence of small objects[1].

3.2.2 Model of the electric response of the passive sensor immersed in an imposed ambient field ϕ_a

The slender geometry of the sensor allows its electric reaction to an applied potential ϕ_a to be modelled as the superimposition of two reactions, which we denote axial and lateral, since they are respectively due to the polarization of the sensor parallel with, and orthogonal to, the sensor axis (see Figure 6). In the model of the axial reaction (see in Figure 6-a) the head electrodes (e_1, e_2) and the tail electrode e_0 respectively centered in $\mathbf{x}_h$ and $\mathbf{x}_t$ are each submitted to the potential $\phi_a(\mathbf{x}_h)$ and $\phi_a(\mathbf{x}_t)$ respectively. As a result, the sensor is axially set under voltage through the potential difference:

$$\Phi_a = \phi_a(\mathbf{x}_t) - \phi_a(\mathbf{x}_h), \tag{7}$$

while the head electrode is submitted to the lateral electric field:

$$E_{a,\perp} = -\boldsymbol{\nabla}\phi_a(\mathbf{x}_h).\mathbf{e}_\perp. \tag{8}$$

where $\mathbf{e}_\perp$ is a unit vector perpendicular to the rostro-caudal axis of the sensor. The first excitation is comparable to the vector of voltages U imposed by the electronics in the active case. Thus, the currents produced by this external polarization are simply given by the model of the active sensor with no objects (1):

$$\mathbf{I}_{ax} = -C^{(0)}\Phi_a, \tag{9}$$

where the minus sign indicates that the sensor has to oppose Φ_a in order to recover its electric balance [Boyer et al., 2012]. The currents produced by the lateral polarization can be modelled by the following relation:

$$\mathbf{I}_{lat} = (1,-1)^T p_\perp E_{a,\perp} = (1,-1)^T I_{lat}, \tag{10}$$

where $p_\perp$ is a scalar named "lateral polarizability" which models how the electric charges laterally distribute on the metal head hemisphere when it is submitted to an electric field (here $-\boldsymbol{\nabla}\phi_a$ as illustrated in Figure 6-b) [Boyer et al., 2012] while I_{lat} denotes the scalar lateral current flowing

[1] An object is small when its size is comparable to that of the sensor thickness.

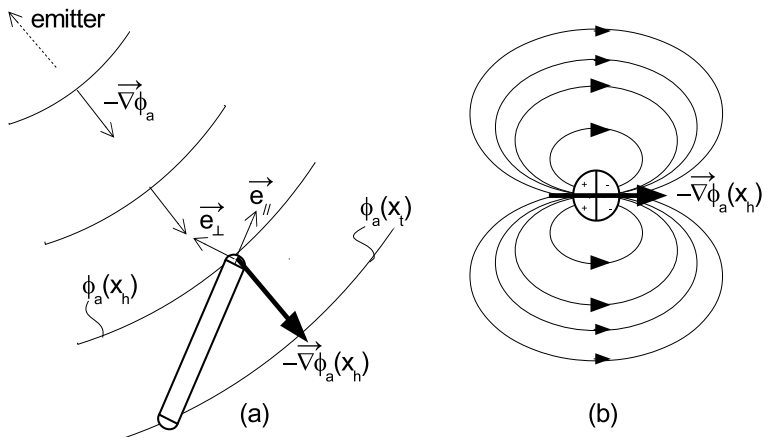

Figure 6: The two components of the currents are produced by different polarizations: **(a) view from above of the axial polarization of the sensor:** the axial currents are produced by the axial polarization of the sensor through the application of a voltage by the iso-potentials applied to the electrodes. **(b) Cross-sectional view of the lateral polarisation of an electrode:** The lateral currents are produced by the lateral polarization of the electrodes by the applied electric field.

across the head electrode. Note that in (10), the $(1,-1)^T$ matrix models the axi-skewsymmetric character of the lateral polarization, the electric charges on one head-electrode being balanced by the opposite charges on the other (see Figure 6-b). Finally, due to the linearity of the physics, the model of currents (5) is given by the following superimposition:

$$\mathbf{I} = \mathbf{I}_{ax} + \mathbf{I}_{lat} \tag{11}$$

where, due to the bilateral (left-right) symmetry of the sensor, the vectors of lateral and axial currents can be easily extracted from the measured currents through the relations:

$$\begin{aligned} \mathbf{I}_{ax} = I_{ax}(+1,+1)^T &= ((I_1+I_2)/2)(+1,+1)^T \\ \mathbf{I}_{lat} = I_{lat}(+1,-1)^T &= ((I_1-I_2)/2)(+1,-1)^T \end{aligned} \tag{12}$$

where I_{ax}, or "axial current", represents the common part of the left and right currents flowing across the two head electrodes e_1 and e_2, while I_{lat} is a "lateral current" representing the differential part of these left and right currents.

3.2.3 Model of the ambient field ϕ_a

The purpose of this subsection is to detail the model of the ambient field ϕ_a of (6) which leads (7-11) to the model of the currents $\mathbf{I}$. The exogenous field $\phi^{(0)}$ is produced by a single source located in $\mathbf{x}_e$ and a set of s sinks modelling the s receiver-electrodes located in $\mathbf{x}_{r,k}$ with $k = 1, 2...s$. Thus, it can be written as:

$$\phi^{(0)}(\mathbf{x}) = \frac{I_e}{4\pi\gamma_0 \parallel \mathbf{x}-\mathbf{x}_e \parallel} + \sum_{k=1}^{k=s} \frac{I_{r,k}}{4\pi\gamma_0 \parallel \mathbf{x}-\mathbf{x}_{r,k} \parallel}, \tag{13}$$

where I_e and the $I_{r,k}$ are the currents which flow out of the emitter, and into the receiver-electrodes, and satisfy the electric charge conservation $I_e + \sum_{k=1}^{k=s} I_{r,k} = 0$. When we consider the expression (6) of ϕ_a, the component $\phi^{(1)}$ is produced by the polarized objects. Let us first remark that when there are several small objects in the scene, the method of reflections of [Boyer et al., 2012] tells us that the effects of the electric influence between objects (secondary and further polarizations) on the measured currents, are negligible compared to those directly produced by their own polarization by $\phi^{(0)}$ (primary polarization). As a result, in the presence of several objects $\mathcal{O}_1, \mathcal{O}_2, ...\mathcal{O}_p$, the measured currents can be directly written as a superimposition of those generated by each of the objects as if it was the only object in the scene, i.e. $\mathbf{I}$ is given by (7-11) where $\phi^{(1)}$ is given by the following superimposition:

$$\phi_a = \phi^{(0)} + \sum_{k=1}^{k=p} \phi_k^{(1)}, \tag{14}$$

where $\phi_k^{(1)}$ represents the electric potential field reflected by the k^{th} object polarized by the imposed external field $\phi^{(0)}$. Because the object is small, $\phi_k^{(1)}$ can be explicitly calculated as [Rasnow, 1996, Boyer et al., 2012]:

$$\phi_k^{(1)}(\mathbf{x}) = -\frac{(\mathbf{x} - \mathbf{x}_k).\mathbf{P}_k.\boldsymbol{\nabla}\phi^{(0)}(\mathbf{x}_k)}{\| \mathbf{x} - \mathbf{x}_k \|^3}, \tag{15}$$

where $\mathbf{P}_k$ represents the polarization tensor of the object $\mathcal{O}_k$ located in $\mathbf{x}_k$. For instance, in the case of spherical objects, the isotropic geometry of the objects does not privilege any polarization direction and we simply have $\mathbf{P}_k = \chi_k a_k^3 \mathbf{1}$, where a_k is the radius of the sphere and $\mathbf{1}$ is the Kronecker tensor while $\chi_k = (\gamma_k - \gamma_0)/(2\gamma_0 - \gamma_k)$ is the contrast factor of the k^{th} object material of conductivity γ_k with respect to the ambient water [Rasnow, 1996]. In particular, when the object is made of an ideal conductive material such as metal, the contrast factor is $\chi_k = 1 > 0$ and its polarization tends to reinforce the ambient field $\phi^{(0)}$ while the electric current lines of the total field ϕ_a are locally funnelled by the object. Meanwhile, when the object is made of an ideal insulating material (e.g. plastic or glass), $\chi_k = -1/2 < 0$ and the object opposes the ambient field. The electric lines of the total field are locally repelled from the object boundaries. Finally, (15) shows that the influence of the object on the sensor becomes comparable to that of the ambient field when its distance from the object is of the order of the object radius a_k.

4 Evaluation of the analytical model

Before addressing the control problem, let us evaluate the previous analytical model of measurements. We used the 3-electrode sensor illustrated in Figure 3-b, together with two external electrodes of a given voltage, as pictured in Figure 7. The two external electrodes produce a potential field $\phi^{(0)}$ as illustrated in Figure 3.a, and a small insulating sphere is positioned between the electrodes. The passive sensor is then translated along a rectilinear path while the currents that penetrate it are recorded. In the conditions of this scenario, **the currents flowing across the measurement electrodes** are computed both on a reference numerical simulator and using the analytical model described in the previous section. The ambient potential ϕ_a given by (14) with (13) computed for two electrodes (one emitter and one receiver) is inserted into the measurements model (7-11) with (15) computed for one insulating object ($\chi = -1/2$) of spherical shape with radius $a = 1$cm. The results are displayed in Figure 8 where the lateral and axial currents of (12) are plotted against the position of the passive probe along its path. A good match between the analytical model and the reference simulator was obtained. The reference simulator runs in-house

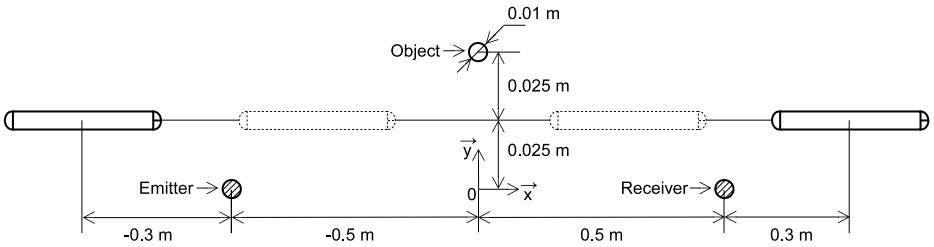

Figure 7: A passive electric probe is translated between two external electrodes (one emitter and one receiver) in the presence of a small insulating sphere.

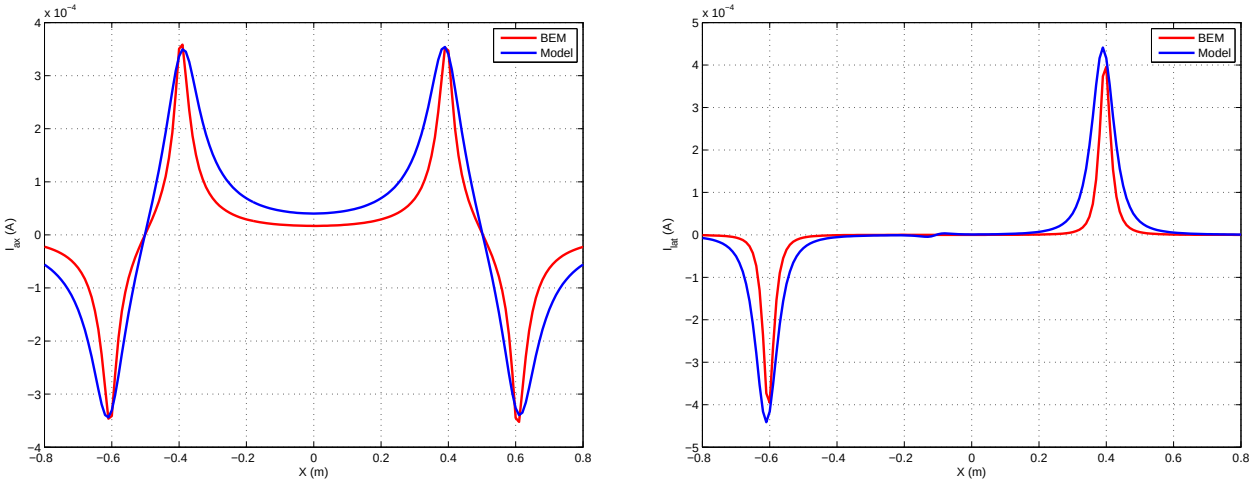

(a) Axial current versus the position of the passive probe along the path.

(b) Lateral current versus the position of the passive probe along the path.

Figure 8: Axial **(a)** and lateral **(b)** currents predicted by the analytical model and the BEM simulation with a two electrode sensor translated between two external electrodes as pictured in Figure 7.

code based on the Boundary Elements Method (BEM). It allows integrating the Laplace equations of the electric potential field (3) without approximation of the boundary geometry (sensor, objects and external electrodes), except those unavoidably introduced by their finite-element meshing. As a result, the discrepancies observed in Figure 8 are due to the reduction process developed in [Boyer et al., 2012] which is essentially based on the method of reflections and the perturbation expansion of the Laplace equations with respect to the aspect ratio of the sensor.

5 Electric feedback-based navigation control

In this section, we introduce the reactive control law which will be used in the rest of the article. The closed loop behavior of the passive sensor in the presence of a single external electrode and a small object is then analysed. The more general case of a passive sensor in the presence of several insulating objects and several external electrodes is then discussed before the description of the experimental implementation in section 6.

5.1 Statement of the problem and control strategy

We want to move the passive sensor with the kinematic control variables (V, Ω) of (2) so that it seeks the exogenous emitter electrode, while avoiding the receivers and any objects, assumed here to be small insulating spheres. To that end, let us first remark that from the laws of electrostatics [Jackson, 1962], the potential field $\phi^{(0)}$ between the external emitter-electrode and the external receiver-electrodes defines a foliation[2] of iso-potential surfaces with maximum values on the emitter boundaries and minimum values on the receivers (all of the receivers being connected to a common ground). This foliation generates an electric field in space which crosses each of the iso-potential folds perpendicularly. As expected, this field and its associated current field (governed by Ohm's law (4)) emanates from the emitter and converges on the receiver. Since all the objects are insulators, they deviate the current lines around their boundaries[3]. Within this basic picture, the control concept consists of considering the passive slender sensor as a vector in a gradient descent like strategy where $-\phi_a(.)$ of (11) is the altitude function. The control law (V, Ω) has to push the sensor toward the global electric potential maximum located on the emitter. To that end, it is first necessary to align the sensor axis with the ambient electric field. This alignment is easy if we recall that in (10) the lateral current I_{lat} is proportional to the lateral projection of the ambient field in $\mathbf{x}_h$ onto the normal axis of the sensor ($\mathbf{e}_\perp$), so aligning the sensor body with the external field is equivalent to null I_{lat}. However, this condition is necessary but not sufficient since, once aligned along the field, the sensor has ascend through the iso-potential folds, up to their global maximum. This second condition is satisfied if the control law ensures that the head is closer to the source than the tail, i.e. if the difference of potentials Φ_a given by (7) is negative, and that the axial current I_{ax} is positive (9). The following feedback control law can ensure these two conditions along with the control objectives:

$$V = V_d \text{ , and: } \Omega = k\frac{I_{lat}}{\mid I_{ax} \mid}. \tag{16}$$

In this equation, k is a strictly positive gain, while $V_d > 0$ denotes a constant positive value that **ensures the sensor goes forward** with a constant axial velocity. This law has been shown to achieve the objective of seeking conductive objects while avoiding insulating ones [Boyer et al., 2013]. However, this was done in the context of active electric sensing in which an active sensor follows the electric lines emitted by the objects polarized by the sensor itself. Going further, **the difference between the present work and active electrosense of [Boyer et al., 2013] can be summarized as follows:**

- **The field followed by the sensor is static. It moves with the sensor in [Boyer et al., 2013].**
- **The field followed by the sensor is generated by a source, i.e. it depends on the distance $r = \parallel \mathbf{x}_h - \mathbf{x}_e \parallel$ between the sensor (its head) and the target, as $1/r$. In the active case [Boyer et al., 2013], the dependence is as $1/r^2$, with r the distance between the sensor's head electrode and the object's center.**
- **And, most critically in active sensing, the electric lines start and end on the targeted object boundaries, while in the passive mode, since the target is a**

[2] In our context, a foliation is a decomposition of the three dimensional space as a union of parallel 2-dimensional submanifolds, or "folds", here defined as the iso-potential surfaces.

[3] In terms of electric potentials, an insulating object generates a local minimum of the potential function ϕ_a.

source (and not a dipole), the electric lines end far from the target (i.e. on the receiver-electrodes). As a result, our electric lines tracking based-strategy could push the sensor far from the target.

In this new context, we are going to analyse the locomotion dynamics (2) controlled by (16), first in the presence of a single source modelling the emitter and second in the presence of a single polarized object. We will then tackle the case of multiple objects and external receivers. This separation is justified by the fact that the electric influence of a source is dominant everywhere except in the vicinity of an object, as mentioned at the end of section 3.2.3. Let us remark that using the formalism of task functions **[Espiau et al., 1992]** with $I_{lat} \to 0$ and $I_{ax} \to I_{ax,d}$ as control objectives and $I_{ax,d}$ being a desired constant value representing the axial current measured by the sensor when its head touches the emitting electrode, one can design other sensor based control laws in which V and Ω are proportional to I_{ax} and I_{lat} respectively. However, the control law (16) has two advantages over these alternatives. Firstly, it avoids the sensor being too slow when it is distant from the target electrode and too fast when it is close to it. Secondly, the ratio $I_{lat}/\mid I_{ax} \mid$ ensures that the sensor's steering is insensitive to the fluctuations of the surrounding fluid conductivity.

5.2 Control analysis of a sensor in the presence of a single source

In this subsection, we analyse the behavior of a passive 3-electrode probe controlled by the feedback law (16) in the presence of a single external electrode. In this case, the electric potential field applied to the sensor is reduced to the first component of (13). We first consider the case of an emitter ($I_e > 0$) and will consider that of a receiver ($I_e < 0$) at the end of the section. In order to localise the external electrode with respect to the sensor, we use the coordinates (ρ, α) of the emitter in a sensor frame centered on the head sensor $(\mathbf{x}_h, \mathbf{e}_\parallel, \mathbf{e}_\perp)$ as indicated in Figure 9-a. Using

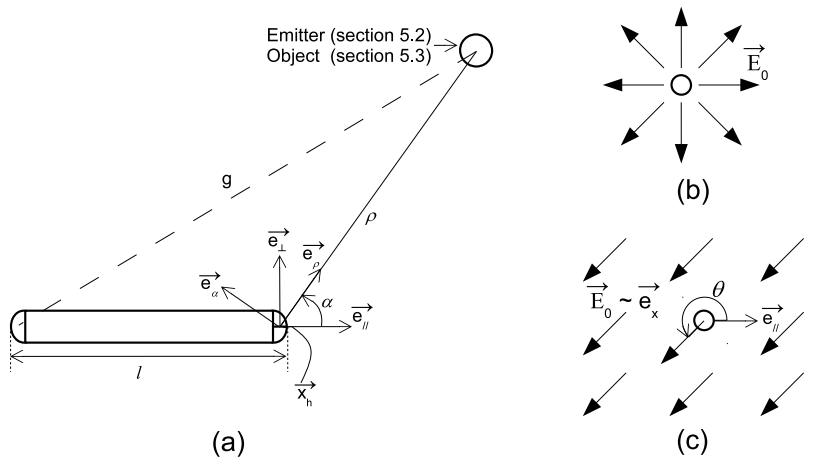

Figure 9: (a) Parametrization of an emitter and a single object in the passive sensor frame. (b) Portrait of the ambient electric field around an emitter, **the ground being at infinity in all directions**. (c) Portrait of the ambient field around a small object**, the ground being at infinity in the direction of $\mathbf{E}_0$.**

these coordinates, the locomotion model (2) of the probe can be rewritten as :

$$\begin{pmatrix} \dot{\rho} \\ \dot{\alpha} \end{pmatrix} = \begin{pmatrix} -\cos\alpha & -\frac{l\sin\alpha}{2} \\ \frac{\sin\alpha}{\rho} & -\frac{l\cos\alpha}{2\rho} - 1 \end{pmatrix} \begin{pmatrix} V \\ \Omega \end{pmatrix}. \tag{17}$$

Now, let us detail the models of axial and lateral currents respectively given by (7-9) and (8-10) in the case where the scene is reduced to a single source emitting the total current I_e. With the notation introduced in Figure 9-a, the sensor is submitted to difference of potential between the tail and the head defined by (13):

$$\Phi_a = \phi_a(\mathbf{x}_t) - \phi_a(\mathbf{x}_h) = \frac{I_e}{4\pi\gamma_0}\left(\frac{1}{g} - \frac{1}{\rho}\right), \tag{18}$$

where $g = (l^2 + \rho^2 + 2l\rho\cos\alpha)^{1/2}$, while the electric exogenous field seen from the head electrode (its center) is simply given by:

$$-\boldsymbol{\nabla}\phi_a(\mathbf{x}_h) = \frac{I_e \mathbf{e}_\rho}{4\pi\gamma_0\rho^2}, \tag{19}$$

with $\mathbf{e}_\rho$ the polar unit vector defined as in Figure 9-a. Introducing (18) and (19) in (9) and (10) respectively, gives:

$$I_{ax} = \frac{C^{(0)} I_e}{4\pi\gamma_0}\left(\frac{1}{\rho} - \frac{1}{g}\right), \tag{20}$$

for the model of the axial currents, and:

$$I_{lat} = \frac{p_\perp I_e \sin\alpha}{4\pi\gamma_0\rho^2}, \tag{21}$$

for the model of lateral currents. Then, inserting (20) and (21) into (16), the control law can be written:

$$V = V_d \text{ , and: } \Omega = k\frac{p_\perp I_e \sin\alpha}{\rho^2 \mid C^{(0)} I_e \left(\frac{1}{\rho} - \frac{1}{g}\right) \mid}. \tag{22}$$

Introducing the control law (22) into (17) gives the closed loop system dynamics governing the passive sensor motion in the field of the source:

$$\begin{pmatrix} \dot\rho \\ \dot\alpha \end{pmatrix} = \begin{pmatrix} -\cos\alpha V - \frac{kA\sin^2\alpha}{2\rho^2|\rho^{-1}-g^{-1}|} \\ \sin\alpha\left(\frac{V}{\rho} - \left(\frac{kA}{\rho^2|\rho^{-1}-g^{-1}|}\right)\left(\frac{l\cos\alpha}{2\rho}+1\right)\right) \end{pmatrix}, \tag{23}$$

where we have introduced the constant value $A = (\mathbf{sign}(I_e)p_\perp/C^{(0)})$. Now, let us remark that the control law (16) is parameterized by the constant linear velocity V_d and the gain k whose the ratio $\zeta = k/V_d$ is a stiffness control parameter which tunes the angular reactivity of the sensor with respect to the speed at which it discovers the front scene. To make ζ explicitly appear in the closed loop dynamics, it suffices to replace the time by $s = Vt$ in (23) and to write:

$$\frac{d}{ds}\begin{pmatrix} \rho \\ \alpha \end{pmatrix} = \begin{pmatrix} -\cos\alpha - \frac{\zeta A\sin^2\alpha}{2\rho^2|\rho^{-1}-g^{-1}|} \\ \sin\alpha\left(\frac{1}{\rho} - \left(\frac{\zeta A}{\rho^2|\rho^{-1}-g^{-1}|}\right)\left(\frac{l\cos\alpha}{2\rho}+1\right)\right) \end{pmatrix}, \tag{24}$$

where geometrically, s represents the distance travelled by the target electrode along its path in the sensor frame. Analysing (24), note that when the sensor is far from the source, ρ is large, and the sensor moves forward in straight line according to the closed-loop dynamics $\frac{d\alpha}{ds} = -\sin\alpha/\rho \simeq 0$, $\frac{d\rho}{ds} = -\cos(\alpha)$. As a result, owing to

the presence of ρ in the denominator of $d\alpha/ds$, the angular reaction of the sensor is low when the source is distant, while its linear velocity is not affected by the distance to the sensor. In practice, when the amplitude of I_{ax} and I_{lat} is too low to be distinguished from the noise, this asymptotic behavior is forced by imposing $\Omega = 0$. When the source is on the bisector of the sensor, i.e. when $g = \rho$, the control law is singular. However, in this case the angular velocity dramatically increases, making the sensor rotate rapidly (with a saturated angular velocity) and escape from the singularity. Apart from these two extreme cases, the control law does ensure the sensor aligns its body with the electric field since in this case, referring to Figure 9-a, $\alpha = 0$ (the sensor head faces the source) or $\alpha = \pi$ (its tail faces the source), are the two equilibrium positions of the angular dynamics, modelled by the second line of (24). Furthermore, when $\alpha \to 0$, the first equation of (24), named "ρ-dynamics" tends to $\frac{d\rho}{ds} = -1$, while when $\alpha \to \pi$, it tends to $\frac{d\rho}{ds} = 1$. As a result, in the first case, the sensor goes towards the external emitter (ρ decreases) while in the second it moves away from it (ρ increases). In line with our control objectives (the sensor goes toward the emitter while facing it), $\alpha = 0$ is a stable orientation of the sensor, while on the contrary, $\alpha = \pi$ is unstable when it is far enough from the emitter. This can be shown by analysing the linearization of the second equation of (24) around $\alpha = 0$ which can be written with $\alpha = \epsilon \simeq 0$:

$$\frac{d\epsilon}{ds} \simeq \frac{\epsilon}{\rho}\left(1 - \left(\frac{\zeta A(\rho + l)}{l}\right)\left(\frac{l}{2\rho} + 1\right)\right), \tag{25}$$

or

$$\frac{d\epsilon}{ds} \simeq \frac{\epsilon}{2l\rho^2}\left(-2A\zeta\rho^2 + \rho l(2 - 3\zeta A) - \zeta A l^2\right). \tag{26}$$

As a result, if $\zeta > (6 - 4\sqrt{2})/A$, the orientation $\alpha = 0$ is stable for any ρ. For the sensor of Figure 4-b, $A = 0.3787$ thus for $\zeta > 0.9061$ the orientation $\alpha = 0$ is stable in the range of detection of the sensor. For lower values of ζ, the orientation is stable for $\rho < \left(2 - 3A\zeta - \sqrt{4 + A^2\zeta^2 - 12A\zeta}\right)/4A\zeta$ which tends to zero with ζ. Thus a large ζ is useful to increase the attractive area. In the second equilibrium position, linearizing (24) around $\alpha = \pi$ (with $\rho > l$ since the sensor's tail faces the source) and using the notation $\alpha = \pi + \epsilon \simeq \pi$, gives:

$$\frac{d\epsilon}{ds} \simeq -\frac{\epsilon}{\rho}\left(1 + \left(\frac{\zeta A(\rho - l)}{l}\right)\left(\frac{l}{2\rho} - 1\right)\right), \tag{27}$$

or

$$\frac{d\epsilon}{ds} \simeq \frac{\epsilon}{2l\rho^2}\left(2\zeta A\rho^2 - \rho l(2 + 3\zeta A) + \zeta A l^2\right). \tag{28}$$

This orientation is unstable for $\rho > l(\frac{2+3A\zeta+\sqrt{4+12A\zeta+A^2\zeta^2}}{4A\zeta})$. When ζ increases the domain of instability increases to include all of the workspace (i.e. $\rho > l$). For any value of ζ, the sensor necessarily reaches the unstable region at a given instant since when the sensor's tail is close to the source (an improbable scenario since the sensor discovers its surrounding environment with its head), the trajectory $(\alpha = \pi, \dot{\rho} = V)$ is stable

and the sensor moves away from the source until the condition of instability becomes satisfied, at which point the sensor turns again to seek the source. Thus we obtain the gradient-like behavior, since when the head sensor faces the electrode ($\alpha = 0$), the sensor is attracted by the electrode (and $1/g < 1/\rho$ and $\Phi_a < 0$), while when the tail faces the electrode $\alpha = \pi$, and the sensor is repelled by the electrode (and $\Phi_a > 0$.)

Finally, when the external electrode is a receiver, $I_e < 0$ and the feedback law (16) reverses the behaviour of the passive sensor, which is then repelled by the receiver. In this case, a similar study can be conducted where $\alpha = 0$ and $\alpha = \pi$ are two equilibrium positions whose stability can be studied with equations (26) and (28) as in the previous case. The results are only modified here by the sign of A which becomes negative. As a result, $\alpha = 0$ is unstable for any $\zeta > 0$ and ρ, and the sensor is repulsed by the insulating object when its head faces the receiver. On the other hand, $\alpha = \pi$ is stable or attractive for any $\zeta > 0$ and $\rho > l$, i.e. when the tail sensor faces the electrode, the control law makes it go away from the emitter with a constant velocity.

Figure 10 illustrates the external electrode paths in the mobile frame of the 3-electrode sensor in Figure 3b. It is obtained by the numerical integration of (24) in both cases where the electrode is an emitter and a receiver, and for a stiff and a soft reactive law with $\zeta = 5$ and $\zeta = 500$ respectively, illustrating in a single picture the entire behavior of the law. As indicated in the illustration, as ζ increases the law is more and more reactive to the target and does ensure attraction toward an emitter and repulsion away from a receiver.

5.3 Control analysis of the sensor in the presence of a single object

In this subsection, we analyse the behaviour of the closed-loop dynamics of the sensor in the vicinity of a small perturbative object, typically a sphere of similar radius to that of the sensor. We first consider an insulating object before moving on to discuss the case of a conductive one. To that end, we examine the simplified case in which a spherical object of radius a is immersed in a uniform field $\mathbf{E}_0 = -\boldsymbol{\nabla}\phi^{(0)}(\mathbf{x}_o)$, where $\mathbf{x}_o$ denotes the sphere's center. This approximation is validated by the fact that the object is small, so its influence on the sensor is limited to a small volume around it, in which $\mathbf{E}_0$ can be considered as uniform and equal to $\mathbf{E}_0(\mathbf{x}_o)$. In contrast to the single external electrode case considered in the previous section (see Figures 9-a and c), the influence of a polarized object such as this, is no longer isotropic. As a result, the movement of the controlled sensor through the scene requires two angles to be parameterized (and not one, as in the previous case). This additional angle parameterizes the position of the sensor with respect to an arbitrarily fixed vector $\mathbf{e}_x$ of the plane of the motion as displayed in Figure 9-c. This angle, denoted θ in (2), is measured with respect to $\mathbf{E}_0$ here, and it is assumed (with no loss of generality) that $\mathbf{E}_0 = E_0\mathbf{e}_x$ (with $E_0 > 0$). In these conditions, using the polar coordinates (ρ, α) of the object location $\mathbf{x}_o$ in the mobile frame attached to the sensor (i.e. the ego-centered parametrization in Figure 9-a), the locomotion model (2) allows the following kinematic model of the scene to be stated:

$$\begin{pmatrix} \dot{\rho} \\ \dot{\alpha} \\ \dot{\theta} \end{pmatrix} = \begin{pmatrix} -\cos\alpha & \frac{l\sin\alpha}{2} \\ -\rho^{-1}\sin\alpha & 1 - \frac{\rho^{-1}\cos\alpha}{2} \\ 0 & 1 \end{pmatrix} \begin{pmatrix} V \\ \Omega \end{pmatrix}. \tag{29}$$

Regarding the electric model of the scene, the applied potential is now given by (14), and $\phi^{(0)} =$

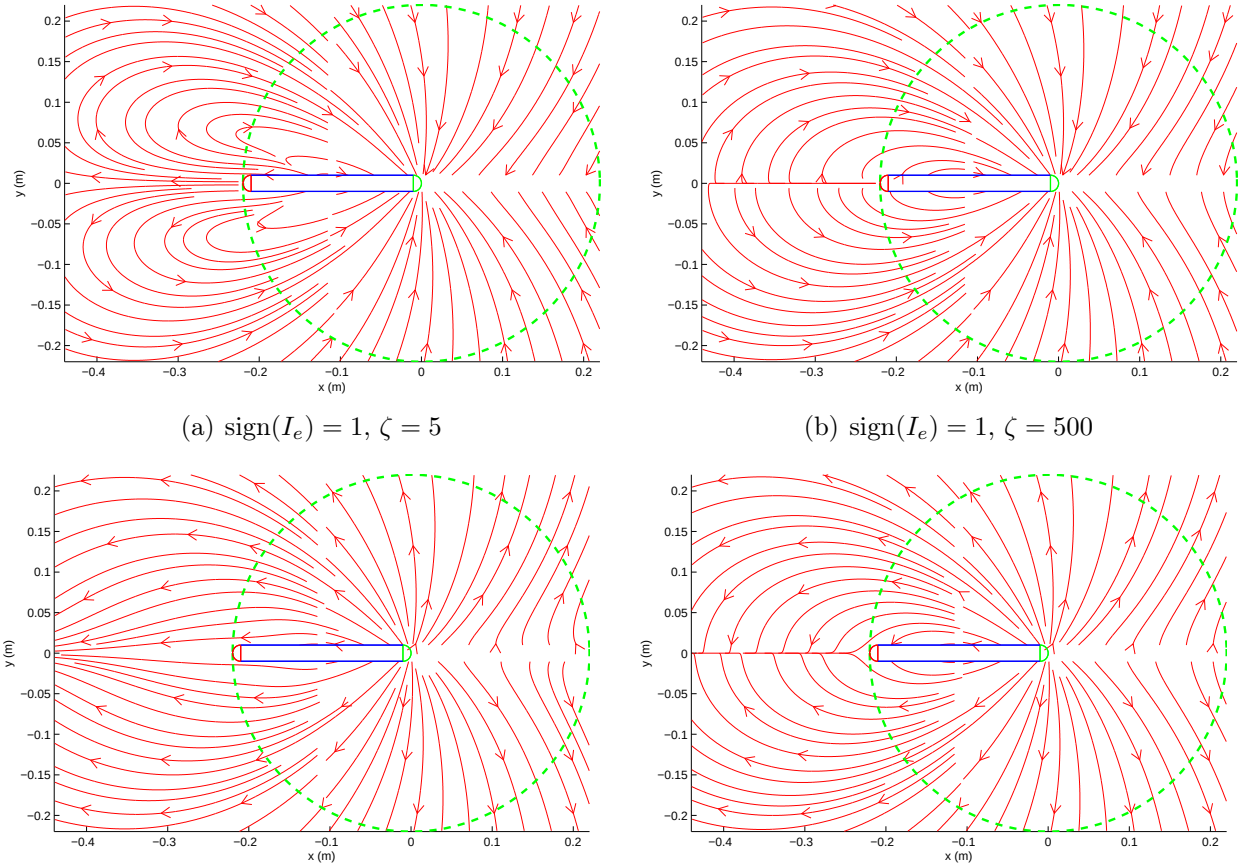

(a) $\mathrm{sign}(I_e) = 1$, $\zeta = 5$

(b) $\mathrm{sign}(I_e) = 1$, $\zeta = 500$

(c) $\mathrm{sign}(I_e) = -1$, $\zeta = 5$

(d) $\mathrm{sign}(I_e) = -1$, $\zeta = 500$

Figure 10: Portrait of the electrode paths in the mobile frame of the sensor **controlled by the reactive law (16) when the electrode is an emitter (a,b) and a receiver (c,d). The circles have a radius one sensor's length. The sensor is attracted (resp. repulsed) by an emitter (resp. a receiver) with a strength which increases with the reactivity parameter** $\zeta = k/V$.

$-\rho \mathbf{e}_\rho.\mathbf{E}_0$ and $\phi^{(1)}$ is given by (15). As a result, we can write:

$$\phi_a = -\rho \mathbf{e}_\rho.\mathbf{E}_0 + \chi a^3 \rho^{-2} \mathbf{e}_\rho.\mathbf{E}_0, \tag{30}$$

from which we derive the applied electric field:

$$-\boldsymbol{\nabla}\phi_a = \mathbf{E}_0 + \chi(a\rho^{-1})^3(2(\mathbf{E}_0.\mathbf{e}_\rho)\mathbf{e}_\rho + (\mathbf{E}_0.\mathbf{e}_\alpha)\mathbf{e}_\alpha). \tag{31}$$

Introducing this electric excitation in the model of currents (9) and (10) gives the model of the measurements in the scene:

$$I_{ax} = -C^{(0)}E_0[l\cos\theta + \chi a^3(\rho^{-2}\cos(\alpha+\theta) - g^{-3}(\rho\cos(\alpha+\theta) - l\cos\theta))], \tag{32}$$

and:

$$I_{lat} = p_\perp E_0[(\chi(a\rho^{-1})^3 + 1)\sin\theta - \chi(a\rho^{-1})^3\cos(\alpha+\theta)\sin\alpha]. \tag{33}$$

Thus, the reactive control law given by (16), can be rewritten in this case as:

$$\Omega = k\frac{p_\perp[(\chi(a\rho^{-1})^3+1)\sin\theta - \chi(a\rho^{-1})^3\cos(\alpha+\theta))\sin\alpha]}{C^{(0)} \mid l\cos\theta + \chi a^3(\rho^{-2}\cos(\alpha+\theta) - g^{-3}(\rho\cos(\alpha+\theta) - l\cos\theta)) \mid}. \tag{34}$$

We will now analyse how the controlled sensor behaves when it approaches the object. To that end, we introduce the steering reactive law (34) into the kinematic model (29), and obtain the closed loop dynamics of the sensor in the scene:

$$\frac{d}{ds}\begin{pmatrix}\rho\\ \alpha\\ \theta\end{pmatrix} \simeq \begin{pmatrix} -\cos\alpha + \frac{l\sin\alpha}{2}\zeta f((\chi(a\rho^{-1})^3+1)\sin\theta - \chi(a\rho^{-1})^3\cos(\alpha+\theta)\sin\alpha) \\ \frac{\sin\alpha}{\rho} - \frac{l\cos\alpha}{(2\rho)}\zeta f((\chi(a\rho^{-1})^3+1)\sin\theta - \chi(a\rho^{-1})^3\cos(\alpha+\theta)\sin\alpha) \\ \zeta f((\chi(a\rho^{-1})^3+1)\sin\theta - \chi(a\rho^{-1})^3\cos(\alpha+\theta)\sin\alpha)\end{pmatrix}, \tag{35}$$

with $f = p_\perp/(C^{(0)} \mid l\cos\theta + \chi a^3(\rho^{-2}\cos(\alpha+\theta) - g^{-3}(\rho\cos(\alpha+\theta) - l\cos\theta)) \mid)$ and $\zeta = k/V$ (which still tunes the stiffness of the steering). This system admits four equilibrium angular states $(\alpha,\theta) = (0,\pi),(\pi,0),(0,0)$ and (π,π). Now, let us remark that when the sensor detects the object, it faces it while following the electric lines of the external emitter $\mathbf{E}_0$ as described in the previous subsection. As a result, with the parametrization of the scene we have chosen, the sensor is initially closed to satisfy $\alpha \in]-\pi/2,\pi/2[$ and $\theta = \pi$, and our analyse is first restricted to the angular equilibrium state $(\alpha,\theta) = (0,\pi)$. The first line of (35) shows that when it is in this angular configuration, the sensor goes toward the object with the ρ-dynamics: $\dot\rho = -V$. Hence, in order to avoid the object, these dynamics should be unstable. To verify that this is actually the case, we linearize (24) around $(\alpha,\theta) = (0,\pi)$ and consider that $\rho \simeq a$ since the influence of the object is non negligible only in a small region near its boundaries. This gives the following linearized angular dynamics, with $\theta = \pi + \epsilon \simeq \pi$, $A = (p_\perp/C^{(0)}l) > 0$:

$$\frac{d}{ds}\begin{pmatrix}\alpha\\ \epsilon\end{pmatrix} \simeq \begin{pmatrix} -\frac{1}{a} - (\frac{l}{2a}+1)\zeta A\chi & (\frac{1}{2a}+1)\zeta A(\chi+1) \\ -\zeta A\chi & \zeta A(\chi+1)\end{pmatrix}\begin{pmatrix}\alpha\\ \epsilon\end{pmatrix}, \tag{36}$$

which has at least one unstable eigenvalue when the object is insulating ($\chi = -1/2 < 0$) and two stable eigenvalues when the object is conductive ($\chi = 1$). As a result, the closed loop dynamics ($\alpha = 0, \theta = \pi, \dot\rho = -V$) are unstable and the sensor is repulsed by the object in the first case ($\chi = -1/2$), while in the second case ($\chi = 1$), the equilibrium dynamics become stable and the sensor is attracted by the object. Finally, as in the single electrode case, this local analysis can be supplemented with a more global one, based on the numerical integration of the nonlinear dynamics (35) and the reconstruction of the object paths which start from initial conditions where $\theta(t_0) = \pi$, $\rho = l$ and $\alpha \in]-\pi/2,\pi/2[$ (the distance of l is beyond the range of detection of the object which is about a, while $\alpha \in]-\pi/2,\pi/2[$ since the sensor discovers the object with its head). Such a representation is displayed in Figure 11. These illustrations, whose the trajectories can intersect due to the projection from the (x,y,θ)-space to the (x,y)-plane, show that the control law does ensure the sensor is repelled by insulating objects an attracted to conductive objects.

We can see that the sensor starts to react when the object is close to its head, i.e. at a distance approximately equal to that of the sensor radius. When the reactivity of the law (tuned by ζ) increases (e.g., when $\zeta = 500$), the sensor deviates quickly but recovers quickly too. A softer control causes the same deviation while eliminating this rebound effect. In the experiments

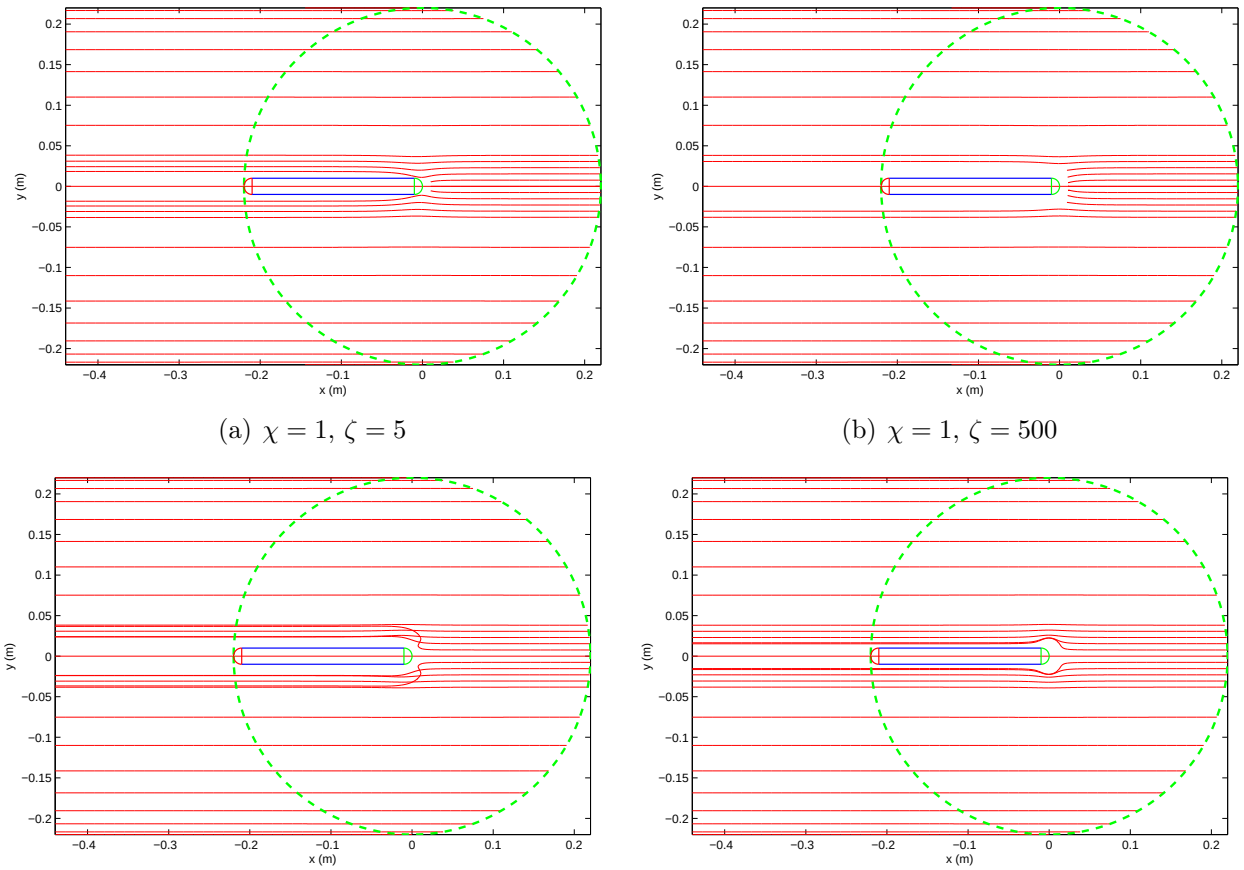

(a) $\chi = 1$, $\zeta = 5$

(b) $\chi = 1$, $\zeta = 500$

(c) $\chi = -1/2$, $\zeta = 5$

(d) $\chi = -1/2$, $\zeta = 500$

Figure 11: Polarized object paths in the mobile frame of the sensor **controlled by the reactive law (16)**. In **(a and b), the object is an ideal conductor (metal) which attracts the sensor and** the paths are interrupted when the object touches the sensor's head. **In (c and d), the object is an ideal insulator (plastic) which repels the sensor. The strength of the reactive law increases with the reactivity parameter $\zeta = k/V$. The dashed circle has a radius of one sensor's length.**

described in section 6, we adopted an average reactivity of $\zeta = 50$, which ensures a smooth reactivity and a stable behavior in the presence of the measurement noise. Finally, in order to assess the influence of the angle θ on the control law, Figure 12 illustrates the object paths when the sensor is not aligned with the ambient field at the initial instant of detection ($\theta(t_0) = 1.8$rad). In this case, the sensor first aligns its body with the field, which bends the paths at their origin, and then avoids the insulating object as in the previous case ($\theta(t_0) = 0$rad).

5.4 Control of the probe in a complex scene

The analysis of the closed loop dynamics of a sensor in the presence of a single external electrode shows that changing the source for a sink (i.e. the emitter electrode for a receiver) changes the sign of I_e, and thus reversing the behavior of the sensor, which is repulsed by the sink. As a result, if we place the sensor among a set of electrodes, one being a source, the others sinks, the additional sinks will increase the efficiency of the law (16) by repelling the sensor towards the target source. Adding objects in the scene causes the sensor to avoid them if they are insulators. Conductive

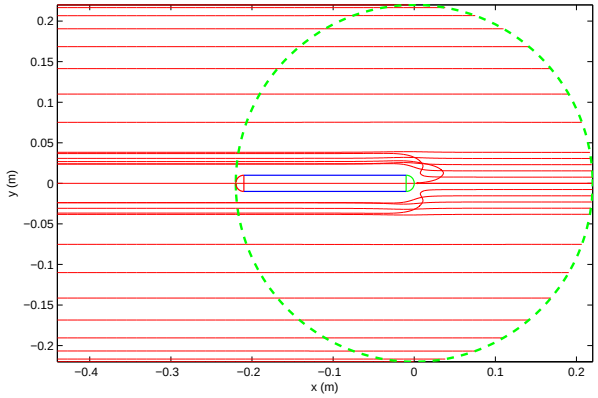

Figure 12: Polarized object paths when the ambient field $\mathbf{E}_0$ is initially not aligned with the sensor ($\theta(t_0) = 1.8$rad). **The object is a small insulating sphere (i.e. $\chi = -1/2$). The reactivity parameter is $\zeta = k/V = 5$. The dashed circle has a radius of one sensor's length.**

objects change the sign of χ, and attract the sensor. Thus we reproduce the behavior of the gradient-like strategy: any insulator object creates a local maximum of $-\phi_a$, while any conductive object generates a local minimum in which the sensor can get stuck. These conclusions are also true for small, non-spherical objects. In the case of insulating objects of large size, for example the walls of a glass tank, the insulators confine the external field ϕ_a and reinforce the attraction of the emitter-electrode, as well see in section 6. In the subsequent experiments, we have concentrate our effort on scenarios with insulating objects. We considered the case of conductive objects in a single experiment and in the discussion.

6 Experimental results

In this second part of the article, we report some experimental results obtained by applying the control law (16) to control the motion of a passive sensor in the presence of an exogenous electric field generated by a set of external electrodes. Some of these experiments are illustrated by attached videos 7. The experimental conditions are those described in section 2, using the 7-electrode illustrated in Figure 2, though only the currents measured by the front head electrodes $\mathbf{I} = (I_1, I_2)^T$ are used. These are decomposed into the axial and lateral currents $I_{ax} = (I_1 + I_2)/2$ and $I_{lat} = (I_1 - I_2)/2$. The conductivity of water is about 380μS/cm, and the external electrodes are metal spheres of radius 0.01m on which a voltage of 10V relative to one another is imposed by a wave generator operating at a frequency of 22.5kHz. Starting from the case of two external electrodes immersed in a tank without any object (experiment 1), we next address the case of a scene containing a plastic ($\chi = -1/2$) or a metal ($\chi = 1$) object (experiment 2), before progressing to the case of several emitters and receivers with several plastic objects (experiment 3). In all these experiments, the control law (16) is applied with the fixed values of the forward constant velocity $V = 0.1$m/s, and the gain of the control law $k = 50.V = 5$, i.e. $\zeta = 50$.

6.1 Seek an emitter-electrode with no object in the scene

We here consider 3 tests for a scene is composed of two external electrodes immersed in the tank illustrated in Figure 5. In the first and second tests, the emitter and the receiver are close to each other and located in one of the corners of the tank (Figures 13 and 14). In the third test,

the two electrodes are located on the opposite sides of the tank (Figure 15(a)). In all the tests, the sensor's path is represented by a dotted lines. The sensor starts from an initial pose also represented by dotted lines; its final pose is marked with a solid line. The letters correspond to intermediate poses in which the measured currents change significantly with time along the path (Figure 13(b)). In test 1, for all initial poses (Figure 13(a)), the current I_{ax} is positive along the path and monotonically increases with time since the initial conditions and the control law ensure that the sensor moves toward iso-potentials ($-\phi_a$) of greater and greater values. On the other hand, I_{lat} converges toward its desired zero-value, possibly changing sign due to the presence of the perturbative repulsive walls (point C) or control law oscillations (point A). When the sensor touches the emitter, I_{ax} rapidly converges towards the (high) value of the current emitted by the target electrode. In the second test, the sensor is initialized in the same position but the emitter is switched between the two electrodes at each trial, as shown in Figure 14, which displays the sensor's path in dotted lines in both cases. In contrast tests 1 and 2, the third test (Figure 15), has the sensor initially located at one side of the tank with its tail facing the emitter, which is positioned at the opposite side of the tank. As expected, the axial current I_{ax} is initially negative until the sensor reorients its head toward the emitter at point A (Figure 15(b)). Beyond this point, the behavior of the robot (and the lateral and axial currents) is similar to tests 1 and 2.

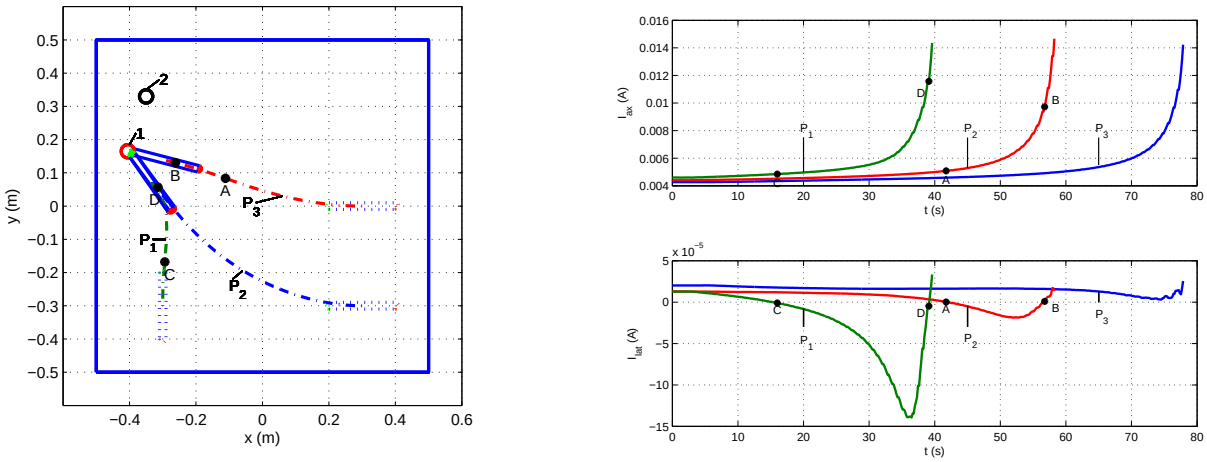

(a) (b)

Figure 13: Test 1: Starting from three different initial poses, the sensor seeks the emitter **until it touches it** following three different paths (P_1, P_2, P_3). (a) Scene and paths of the sensor **with (P_1) and without (P_2) perturbative object**. **The emitter (resp. the receiver) is represented by the sphere numbered 1 (resp. 2). The initial (final) poses are shown in dashed (solid) line.** (b-above) Axial and (b-below) lateral current I_{ax} and I_{lat} for the three **different** paths ($P_{1,2,3}$) along which the currents are measured, **A, B, C, D indicate poses where the sign of lateral currents change**.

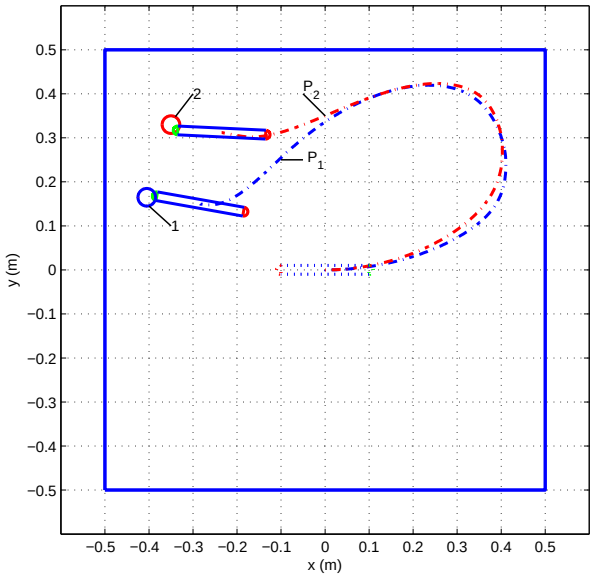

Figure 14: Test 2: The sensor seeks the emitter which is switched between the two electrodes. **The initial pose of the sensor is shown in dashed line while its final poses are shown by the solid line. Spheres 1 and 2 represent the emitter and receiver. The path P_1 (resp. P_2) is that followed by the sensor when the spherical electrode 1 (resp. 2) is the emitter, the other being the receiver.**

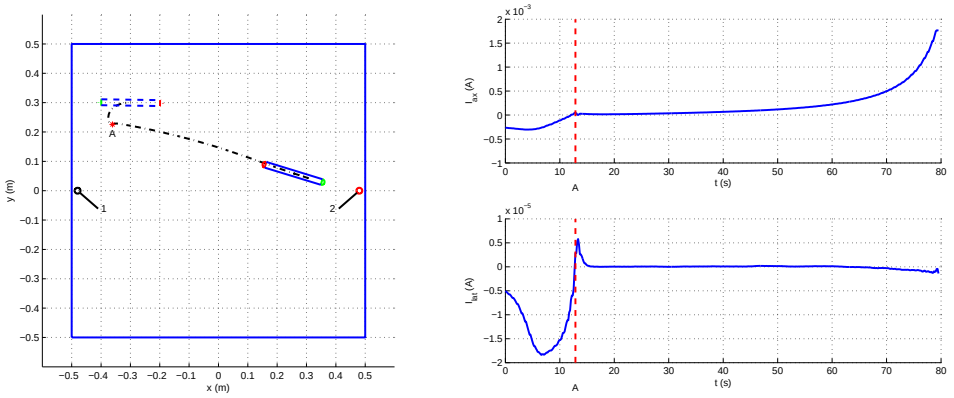

(a) (b)

Figure 15: Test 3: The sensor seeks the emitter starting from an initial pose with its tail facing the emitter. (a) Scene and path of the sensor. **The final (initial) pose is shown in solid (dashed) line. Sphere 1 represents the receiver; sphere 2 is the emitter. (b-above) Axial current I_{ax}. (b-below) Lateral current I_{lat}. The letter A indicates the pose in which, the axial current changes sign while tilting its head toward the emitter.**

6.2 Seek an emitter-electrode in the presence of one object

In this experiment, the scene is composed of two external electrodes positioned on two opposite sides of the tank. An object is immersed between them. In the first test (test 1), the object is insulating (a plastic cylinder), in the second test (test 2) conductive (copper tube). The test is repeated after having removed the object from the scene to assess the effect of the object (Figure

16). In the case with no object, we observe the same behaviors as those discussed in the previous section. As expected, the insulating object deviates the external electric field lines, causing the sensor to avoid the object. This phenomenon is illustrated in Figure 16(b) between points A and E. Before point A and after point E, the robot recreates the behavior observed in the no-object tests since the influence of the object is negligible compared to that of the ambient exogenous field. Between point A and B, the robot detects the presence of the object on its left-hand side ($I_{ax} > 0$ and $I_{lat} > 0$), and turns to the right to avoid it. Between points A and C, the current I_{ax} decreases due to the proximity of the resistive object to the sensor head (between A and C) and tail (C and D) electrodes.

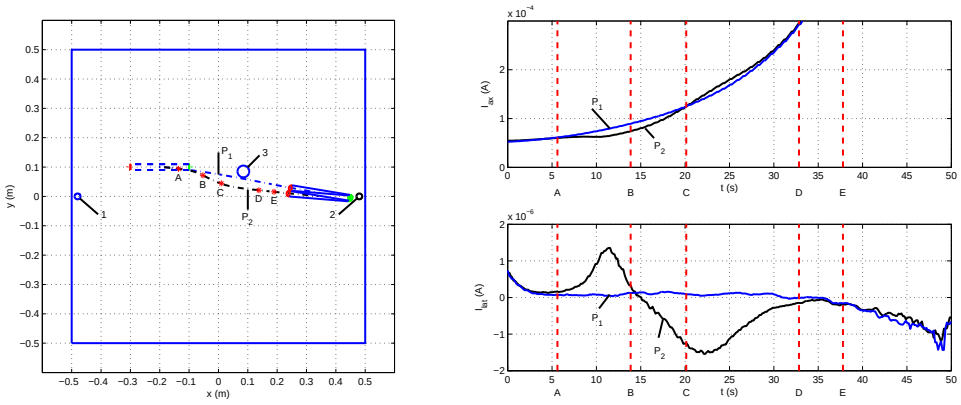

(a) (b)

Figure 16: Test 1: The sensor seeks the external emitter while avoiding an insulating (spherical) obstacle placed in its path. (a) Scene and path of the sensor. **The perturbative insulating sphere is numbered 3. The initial (final) pose is shown in dashed (solid) line. The receiver and the emitter are indicated by small spheres numbered 1 and 2 respectively.** (b-above) Axial and (b-below) lateral currents I_{ax} and I_{lat} measured along the path P_2 with the object, and along P_1 without object. **A, B, C, D, E represent some poses and their associated measured currents mentioned in the text.**

In the second test (Figure 17), with a conductive object, the sensor starts its trajectory as though there were no object, but then suddenly deviates from that trajectory and gets stuck beside the object. This is naturally explained by the fact that the conductive object locally funnels the ambient electric lines which steer the sensor toward the object. From the gradient-like point of view, the conductive object generates a local minimum of $-\phi_a$ into which the sensor falls.

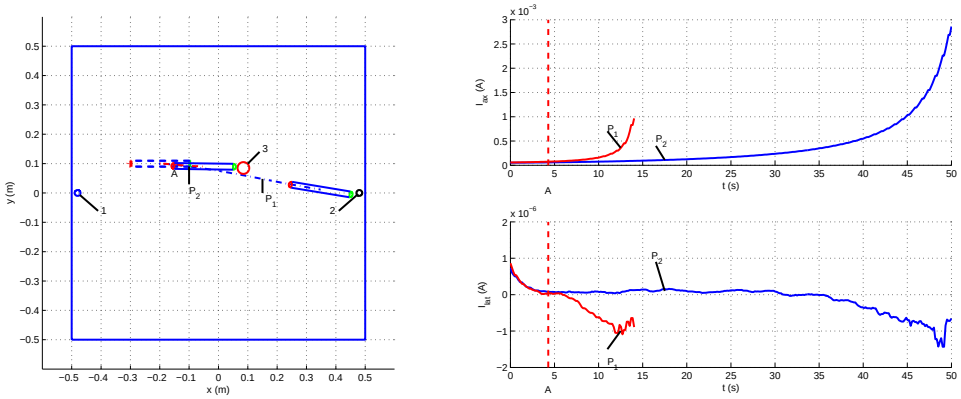

(a) (b)

Figure 17: Test 2: The sensor seeks the external emitter but is locally attracted by a (spherical) conductive object **placed in its path**. (a) Scene and path of the sensor **with (P_2) and without (P_1) the object. The conducting sphere is numbered 3. The receiver and the emitter are indicated by small spheres numbered 1 and 2 respectively. The initial (final) pose is shown in dashed (solid) line.** (b-top) Axial and (b-bottom) lateral current I_{ax} and I_{lat} measured along the path with the object (P_2), and without (P_1) the object. **A indicates the pose at which the probe detects the object and changes its path to seek it.**

6.3 Navigation of a passive sensor in a moving external electric field with and without objects

In this subsection, we consider a case with several external electrodes. One is an emitter, another is a receiver while all the others are electrically disconnected from the emitter-receiver pair and can be considered as small conductive objects. The configuration of the emitter-receiver can be switched manually. It generates an ambient electric field flowing through the scene whose the configuration changes over time in response to the emitter-receiver switches. The first test (test 1) deals with the case in which there is no object in the scene (Figure 18). In the second, several insulating objects are added to the scene (Figure 19). In Figure (18(a)), the sensor paths are numbered with the same number as that of the active emitter electrode. The receiver is the electrode immediately anti-clockwise to the emitter electrode. These successive commutations thus generate a discontinuous turning field in the scene. This explains the discontinuities observed on the axial and lateral currents in Figure (18(b)). As shown in Figure (18(a)), the sensor tries to seek a moving emitter that it never reaches and is steered by the exogenous controlled field. The result is that the sensor revolves around the tank. As expected from the control law, between each commutation, the axial currents tends to recover their positive sign. On the other hand, the commutations are too close in time for the lateral currents to recover their zero value. This **is explained by the fact** that the sensor has not enough time to realign its body on the external field between any two commutation events.

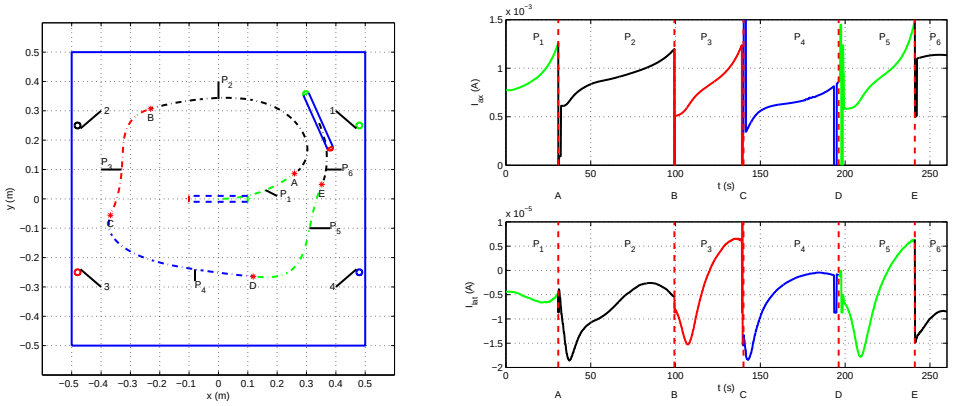

(a) (b)

Figure 18: Test 1: The sensor tries to follow the electric lines of a discontinuous time-varying electric field. **The rotation of the electric field is obtained by switching emission between four electrodes.** (a) Scene and path of the sensor. **The electrodes are indicated by small spheres numbered 1, 2, 3, 4. The initial (final) pose of the probe is shown in dashed (solid) line. Letters A, B, C, D, E indicate the poses at which the emission is switched from one electrode to another. The sensor paths P_1 (from initial pose to A), P_2 (from A to B), P_3 (from B to C), P_4 (from C to D), P_5 (from D to E) and P_6 (from E to final pose) are numbered according to the external electrode which is activated except P_5 and P_6 which corresponds to the activation of electrode 1 and 2 respectively (the activation being cyclic).** (b-above) Axial and (b-below) lateral current I_{ax} and I_{lat} recorded along the paths $P_{1,2,3,4,5,6}$ with electrodes 1,2,3,4,1,2 activated respectively with discontinuities at the switching instants A, B, C, D, E.

In a second test (test 2), we considered the same scene in which we immersed 5 insulating objects (plastic cylinders) (Figure 19(a)). The sensor is initially located at the center of the tank with its head oriented toward the emitter. The electric activity of the external electrodes is the same as in the previous test. The sensor still tries to catch up the turning field while slaloming between the insulating objects, avoiding them all, as is shown in Figure (19(a)). The presence of the insulating objects perturbs the axial current locally which consequently changes sign, similar to the test where the head sensor was close to the insulating wall (test 2 of experiment 1).

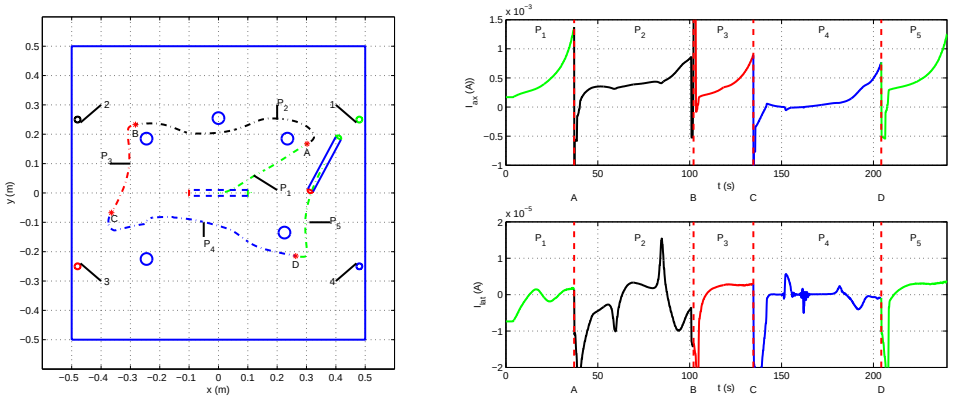

(a) (b)

Figure 19: Test 2: The scene is composed of a set of insulating spherical objects (not numbered) **placed in a rotating field. The rotation of the electric field is obtained by switching between four electrodes numbered 1, 2, 3, 4. (a) Scene and path of the sensor. The initial (final) pose of the probe is shown in dashed (solid) line. Letters A, B, C, D indicate the poses at which the emission is switched from one electrode to another. The sensor paths P_1 (from initial pose to A), P_2 (from A to B), P_3 (from B to C), P_4 (from C to D), P_5 (from D to final pose) are numbered according to the emitting electrode except P_5 for which electrode 1 is the emitter. Axial (b-above) and lateral (b-below) currents I_{ax} and I_{lat} measured along the paths P_1, P_2, P_3, P_4 and P_5 with discontinuities at the switching instants.**

7 Discussion and perspectives for future research

This article addresses the problem of underwater navigation in confined environments by sensing external electric fields. It is based on a sensor [Servagent et al., 2013] inspired by a mode of perception used by many electric fish species. The sensor's control approach is reactive and does not require any model to be implemented. Based on tracking electric current lines, it allows a motion controlled probe to seek an emitting external electrode while avoiding receivers and insulating objects. One obvious application of this work would be in the design of docking devices for future generation of AUVs. Figure 20 illustrates principles of such a potential electric docking station. In particular 20.c shows a device composed of a set of receiver electrodes arranged in a space bounded by insulating walls which confine and shape the electric field, all whose electric field lines converge toward a single emitter electrode located in the docking point. Applying the control strategy outlined in this article, the AUV would follow the electric lines until it touched the emitter, before mechanical anchoring. This electric device could be used as an intermediate phase before mechanical docking, after the AUV has been attracted by a larger range sensor as sonar. In order to apply the control strategy proposed in the article to a realistic AUV, several issues remain to be addressed.

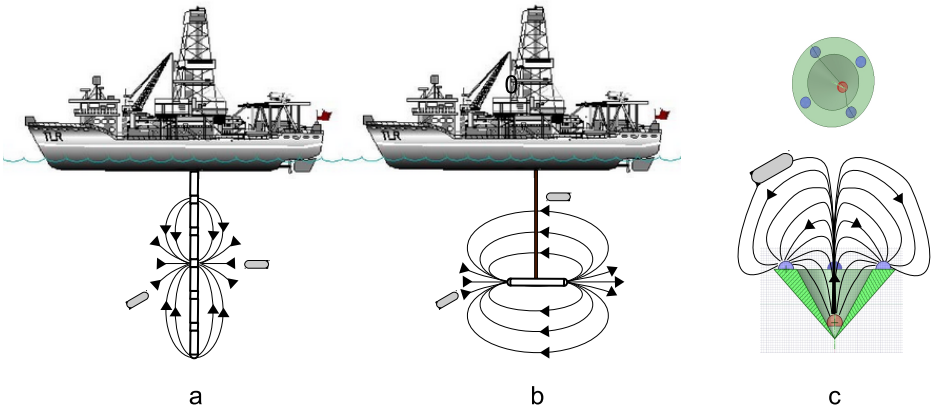

Figure 20: Outline schematic of electric docking stations. (a) An immersed vertical pole on which are arranged a set of electrodes set under controlled voltages in order to attract the AUVs for recharging their batteries. (b) This docking station is directly inspired from the probes design of the article. It could be yaw controlled in order to help docking. (c) An insulating nozzle confines the electric current lines which flow from the emitter (at the top of the cone) to a set of receivers located at the entrance to the nozzle. This field of electric lines could steer an AUV towards the emitter where the docking can be achieved by an anchoring mechanical device.

Firstly, we need to assess to which extent the control strategy is dependent on the morphology of our slender probes. While the low aspect ratio of the slender probes is required to allow the robot to sense the ambient field without perturbing it too much, this condition should be preserved for any AUV with a laterally compressed shape, since in this case the lateral currents would be representative of the lateral flux of the external field. However, the lateral (left-right) symmetry of the electrodes with respect to the rostro-caudal axis of the robot would have to be respected. We have already implemented such a reactive control strategy on the first autonomous underwater robot equipped with electric sense. Named ANGELS, this robot is a reconfigurable swimming anguilliform robot composed of a set of detachable rigid modules controlled by propellers, which navigate using the electric sense (see Figure 2). In a EU-funded project, we addressed the issue of the docking of two modules. Figure 21 shows several photos extracted from a video (`http://www.youtube.com/watch?v=0dVc3JrIds0`). In this video, a module navigates in passive mode while another module is at rest and electrically active, producing an electric field in its surrounding. Using the proposed reactive control strategy, the passive module follows the electric current lines of the active module until it touches its tail, where a mechanical docking device was located. This experiment shows that the control approach in this article is applicable to a wider range of morphologies than that of our slender probes.

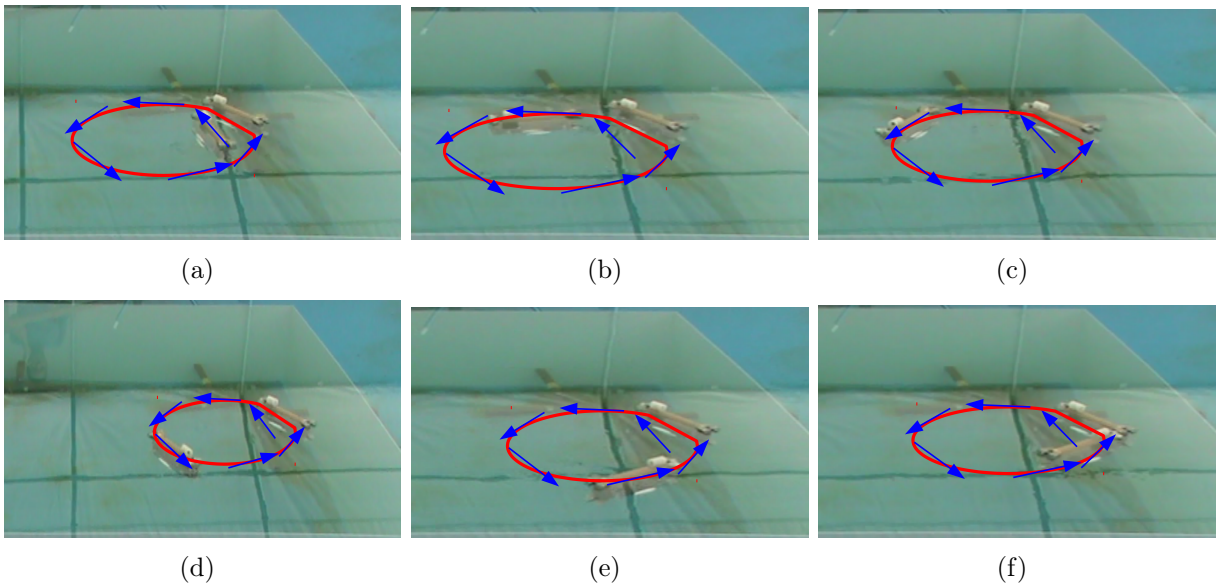

Figure 21: Docking of two modules of the reconfigurable anguilliform robot ANGELS: The passive module seeks the emitter of the active module by following the electric current lines generated by the polarization of the active module with the reactive law (16). The trajectory followed by the passive module is indicated by a solid line with arrows indicating the direction of the movement. (a) At the initial time, the two modules are in a parallel configuration. (b,c,d,e) The passive module turns around in order to seek the emitter of the active module till touching its tail (f).

Another critical issue is that of the local minima generated by conductive objects, upon which the AUV could get stuck before reaching the docking point. One solution might consist in giving the AUV the ability to distinguish the primary electric field generated by the emitter and the secondary field generated by the polarization (by the primary field) of any conductive object. If the conductive object is small, the secondary field that it reflects is that of a dipole falling off as $1/r^2$, compared to the field generated by the source (emitter) which falls off as $1/r$. Based on this, a possible solution would be to use the intermediate or "neck" electrodes between the head and the tail to measure how the electric field decreases along the sensor. For instance, in the case of the 7-electrode slender probe in Figure 2, if the axial currents measured by two rings of electrodes separated by a distance d decrease as $1/d$ the field is produced by a source, i.e. by the emitter, and the sensor should be attracted, but if the axial currents decrease as $1/d^2$, the field is that of a dipole (i.e. a conductive object) and the sensor should ignore it. **Although valuable for small conductive objects (for which the electric response falls off as $1/r^2$), this approach would fail for large objects whose response falls off as $1/r$. As a result, though it is unlikely for docking applications for which the path to the emitter can be legitimately assumed to be cleared of any objects (i.e. perturbed by water turbidity only), if by accident a large object (such as a large metal plate) would approach the emitter, though not come so close that it obstructed the passage to the docking point, alternative strategies would have to be developed. One promising strategy, which would tackle the case of both small and large conductive perturbative objects, would consist of taking advantage of the linearity of the physics of electric sense (equations (3) and (4)) to superimpose passive and active electric sense feedback controllers working at different emission frequencies. In this case, the voltage set between the two poles of the sensor (mounted on the AUV) would be the superimposition of two components,**

one generated by the external field (through an external wave voltage generator fixed to the docking station), the other produced by a voltage wave generator mounted on the AUV. Then, assigning different frequencies ω_p and ω_a to the external and AUV-mounted generators respectively, would generate currents with two harmonics of the same frequency, that can be used in a feed-back law of the form (with $k_p > 0$ and $k_a < 0$):

$$V = V_d \ , \ \Omega = k_p \frac{I_{lat}(\omega_p)}{\mid I_{ax}(\omega_p) \mid} + k_a \frac{I_{lat}(\omega_a)}{(I_{ax} - I_{ax}^{(0)})(\omega_a)}, \tag{37}$$

with $I_{ax}^{(0)}$, the axial current with no object nearby. We recognize the feedback law (16) in the first component of (37). This ensures the vehicle seeks the external emitter and avoid the insulating objects, while the second component has been proposed in [Boyer et al., 2013] where it is shown to ensure the vehicle avoids any contrasted object (including conductors). This law would ensure that the AUV avoids both conductive and insulating perturbative objects while seeking the emitter. In particular, when the AUV approaches the external emitter, the current flowing out of the fixed emitter becomes perturbed by the field of the AUV, and the two components of (37) compete. Thus, if the docking station is equipped with a device allowing it to detect the presence of the AUV through the presence of a current of frequency ω_a, the station can emit a signal (e.g. a current with a third frequency ω_c, the index "c" meaning "communication"), which, when detected by the AUV, makes it remove the repulsive active feedback term ($k_a = 0$), and permits the docking.

Finally, while all experiments have been performed using tap water and a homogeneous low conductivity hypothesis, most of the possible applications for docking are related to oceans and salt turbid water with conductivity heterogeneities. In these more challenging situations, we start by discussing the case of homogeneous salt water before evoking the case of heterogeneities. Salty water is about 100 times more conductive than fresh water. To consider the consequence of such a change on the techniques described so far, let us consider the representative example of figure 4(a) (i.e. one emitter and one receiver with a single passive sensor moving between them). In these conditions, the imposed external voltage U_e set between the emitter and the receiver, and the external current I_e flowing out of the emitter are related through the Ohm's law:

$$I_e = C_{ext} U_e, \tag{38}$$

with $C_{ext} = \gamma_0 S_{ext}$ denoting the conductance of the scene between the two external electrodes with no sensor in it. This depends on the geometry (through the factor S_{ext} function of the distance between the emitter and the receiver) and the water's conductivity γ_0. Maintaining a given power of emission $P_e = U_e I_e = C_{ext} U_e^2$, while shifting from fresh to sea water through $\gamma = \alpha\gamma_0$ (with $\alpha = 100$ in case of sea water), U_e becomes $U_e/\sqrt{\alpha}$, while I_e varies as $\sqrt{\alpha} I_e$ from (38). Finally, exploiting the fact that $p_\perp = \gamma_0 s_\perp$ and $C^{(0)} = \gamma_0 S^{(0)}$ with $s_\perp$ and $S^{(0)}$ depending on the sensor geometry only [Boyer et al., 2012], equations (9), (10) and (13) of the article show that the responses I_{ax} and I_{lat} are multiplied by $\sqrt{\alpha}$. As a result for a given power, if γ is multiplied by 100, U_e is divided by 10 and I_{ax}, I_{lat} are multiplied by 10, but since the control law (16) feeds back the ratio $I_{lat}/ \mid I_{ax} \mid$, it is not affected by the change of conductivity.

As regards the sensing range, it is conditioned by the physics (electrokinetics) and the emitting-receiving electronics. Considering only physics, the range is defined as the distance to the emitter at which the minimum values of I_{ax} and I_{lat} are detected by the sensor. Using this definition in (20) and (21) shows that the sensing range is increased by a factor of the order of $(\alpha)^{1/4}$ (the axial range, i.e. related to I_{ax}, is in reality increased by a higher factor). In short, based on physics only, the sensing range in sea water should be multiplied by 3. However, the drop of the emitted voltage U_e decreases the signal/noise ratio of our emitting electronics (dedicated to fresh water) and decreases the sensing range. This has been observed in the active case where U_e is no longer imposed by an external device (emitter - receivers) but rather by the sensor itself. In this case, we shown in [Servagent et al., 2013] that recalibrating the reception electronics allows limiting the drop of sensitivity (which shifts from $\pm 0.1\%$ to $\pm 0.5\%$). To maintain exactly the same performance as in the fresh water, a direct way would be to redesign the emitting electronics with a generator capable of generating a regular high current for a reasonable voltage. Another solution would be to change the geometry of the sensor in order to decrease its external conductance (modelled by $C^{(0)}$ and $p_\perp$) through the terms $s_\perp$ and $S^{(0)}$, to compensate for the increase in water conductivity.

In turbid, but homogeneous water (i.e. with an homogeneous concentration of particles), only the conductivity is affected and the previous context is preserved. This has been experimentally observed for waters to which coffee powder or highly viscous mud (with bentonite) has been added. Preliminary experiments show that the electric sense works well here too. Exhaustive assessment of the techniques for a conductivity that varies in space and time will require further experiments subject of a future work. To introduce this future study, we can emulate the effect of electric nontransparent particles by modelling each of them as a sphere as outlined in section 3.2. Figure 22 displays the simulation of a passive sensor controlled with the reactive law (16) in the presence of an active sensor (playing the role of the docking station) and of such electric inhomogeneities randomly distributed in space with concentrations $N_1 = 25$, $N_2 = 50$ and $N_3 = 75$ particles/m^2. The inhomogeneities are defined by two populations of particles, one of conductive spheres with a contrast factor $\chi = +0.1$ or $\chi = +0.5$, the other of insulating ones ($\chi = -0.1$ or $\chi = -0.5$). These values of the contrast factor correspond to a shift of water conductivity of $\pm 40\%$ ($\chi = \pm 0.1$) and $\pm 300\%$ ($\chi = \pm 0.5$). The results displayed in Figure 22 are statistically representative of the trends observed on a high number of trials.

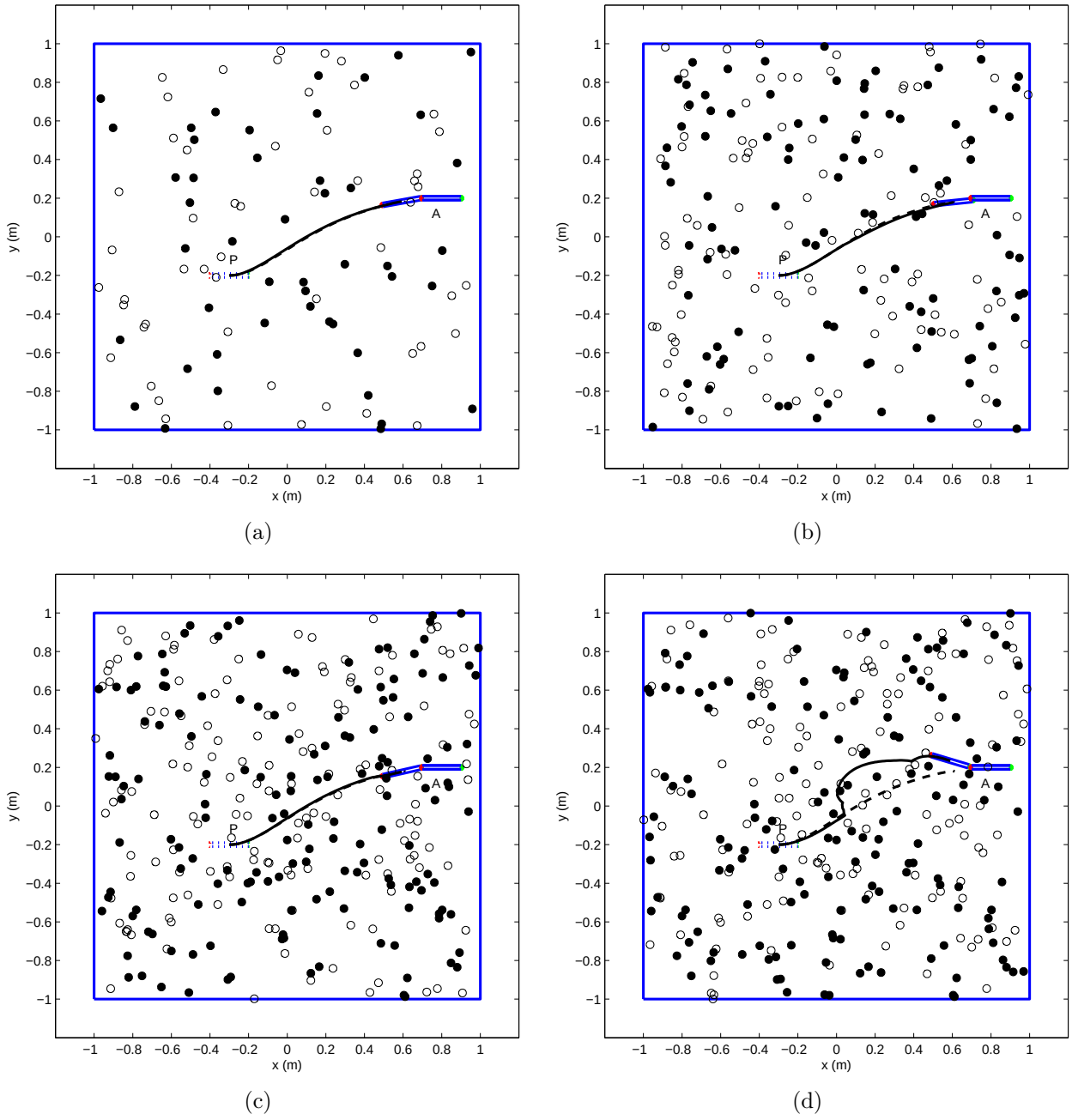

Figure 22: **Simulation of the docking of two probes in presence of electric inhomogeneities. The inhomogeneities are modelled as small spheres of radius $a = 0.02$m. Some of them (in grey) are insulating with a contrast factor $\chi = -0.1$ (a,b,c) and $\chi = -0.5$ (d), the others (in black) are conductive with $\chi = 0.1$ (a,b,c) and $\chi = 0.5$ (d). The concentration of inhomogeneities is (a) $N = 25$ particles/m^2, (b) $N = 50$ particles/m^2, (c,d) $N = 75$ particles/m^2. One of the two probes (P) is passive and controlled with the feedback law (16), while the second (A) is active and steady. The first probe plays the role of the AUV, the second that of the docking station. The initial (final) pose of the passive probe is indicated in dashed (solid) line. The path with (without) inhomogeneities is drawn in solid (dashed) line.**

These preliminary results show that the control law remains robust to an inhomo-

geneous distribution of electric conductivity. In particular, though the path of the sensor is more and more deviated as the concentration and the electric contrast of inhomogeneities increase, the control objective (seek the emitter) is preserved in all cases.

Acknowledgment

The authors gratefully acknowledge the reviewers' comments, and thank Douglas Carnall for his careful proofreading of this manuscript.

Appendix A: Index to Multimedia Extensions

The multimedia extensions to this article are at: http://www.ijrr.org.

Extension	Type	Description
1	Video	Video of the experiments

References

[Baffet et al., 2008] Baffet, G., Gossiaux, P., Porez, M., and Boyer, F. (2008). Underwater robotics: localization with electrolocation for collision avoidance. In *Proceedings of CIFA*.

[Boyer et al., 2012] Boyer, F., Gossiaux, P., Jawad, B., Lebastard, V., and M.Porez. (2012). Model for a sensor bio-inspired from electric fish. *IEEE transactions on robotics*, 28(2):492–505.

[Boyer and Lebastard, 2012] Boyer, F. and Lebastard, V. (2012). Exploration of objects by an underwater robot with electric sense. In Prescott, T., Lepora, N., Mura, A., and Verschure, P., editors, *Biomimetic and Biohybrid Systems*, volume 7375 of *Lecture Notes in Computer Science*, pages 50–61. Springer Berlin Heidelberg.

[Boyer et al., 2013] Boyer, F., Lebastard, V., Chevallereau, C., and Servagent, N. (2013). Underwater reflex navigation in confined environment based on electric sense. *IEEE Transactions on Robotics*, 29(4):945–956.

[Brignone et al., 2007] Brignone, L., Perrier, M., and Viala, C. (2007). A fully autonomous docking strategy for intervention auvs. In *IEEE Oceans 2007*.

[Bullock and Heiligenberg, 1986] Bullock, T. and Heiligenberg, W. (1986). *Electroreception*. Wiley.

[Chevallereau et al., 2012] Chevallereau, C., Boyer, F., Lebastard, V., and Benhachenhou, M. (2012). Electric sensor based control for underwater multi-agents navigation in formation. In *IEEE Conference on Robotics and Automation,*.

[Davis and Hopkins, 1988] Davis, E. and Hopkins, C. D. (1988). Behavioural analysis of electric signal localization in the electric fish, gymnotus carapo , gymnotiformes. *Animal Behaviour*, 36(6):1658–1671.

[Emde et al., 1998] Emde, G. V. D., Schwarz, S., Gomez, L., Budelli, R., and Grant, K. (1998). Electric fish measure distance in the dark. *Letters to Nature, Nature*, 395:890–894.

[Espiau et al., 1992] Espiau, B., Chaumette, F., and Rives, P. (1992). A new approach to visual servoing in robotics. *IEEE Transactions on Robotics and Automation*, 8(3):313–326.

[Feezor et al., 2001] Feezor, M. D., Sorrell, F. Y., Blankinship, P. R., and Bellingham, J. G. (2001). Autonomous underwater vehicle homing/docking via electromagnetic guidance. *IEEE Journal of Oceanic Engineering*, 4:1137 – 1142.

[Happel and Brenner, 1965] Happel, J. and Brenner, H. (1965). *Low Reynolds number hydrodynamics*. Prentice Hall.

[Hobson et al., 2007] Hobson, B. W., McEwen, R. S., Erickson, J., Hoover, T., McBride, L., Shane, F., and Bellingham, J. G. (Sept. 29 2007-Oct. 4 2007). The development and ocean testing of an auv docking station for a 21" auv. *OCEANS 2007*, pages 1–6.

[Hopkins, 2009] Hopkins, C. D. (2009). Electrical perception and communication. In *Encyclopedia of Neuroscience*, volume 3, pages 813–831. Oxford: Academic Press, New York.

[Jackson, 1962] Jackson, J. (1962). *Classical Electrodynamics*.

[Kalmijn, 1966] Kalmijn, A. (1966). Electro-perception in sharks and rays. *Nature*, 212(5067):1232–1233.

[Knight et al., 1981] Knight, W., Pridham, R. G., and Kay, S. (1981). Digital signal processing for sonar. *Proceedings of the IEEE*, 69(11):1451–1506.

[Kondo et al., 2012] Kondo, H., Okayama, K., Choi, J.-K., Hotta, T., Kondo, M., Okazaki, T., Singh, H., Chao, Z., Nitadori, K., Igarashi, M., and Fukuchi, T. (21-24 May 2012). Passive acoustic and optical guidance for underwater vehicles. *OCEANS, 2012 - Yeosu*, pages 1–6.

[Krupinski et al., 2008] Krupinski, S., Maurelli, F., Grenon, G., and Petillot, Y. (15-18 Sept. 2008). Investigation of autonomous docking strategies for robotic operation on intervention panels. *OCEANS 2008*, pages 1–10.

[Lebastard et al., 2012] Lebastard, V., Boyer, F., Chevallereau, C., and Servagent, N. (2012). Underwater electro-navigation in the dark. In *IEEE Conference on Robotics and Automattion*.

[Lebastard et al., 2010] Lebastard, V., Chevallereau, C., Amrouche, A., Jawad, B., Girin, A., Boyer, F., and Gossiaux, P. (2010). Underwater robot navigation around a sphere using electrolocation sense and kalman filter. In *IROS 2010 IEEE*.

[Lee et al., 2002] Lee, P.-M., Jeon, B.-H., and Lee, C.-M. (29-31 Oct. 2002). A docking and control system for an autonomous underwater vehicle. *OCEANS '02 MTS/IEEE*, 3:1609–1614 vol.3.

[MacIver et al., 2004] MacIver, M., Fontaine, E., and Burdick, J. (2004). Designing future underwater vehicles: principles and mechanisms of the weakly electric fish. *IEEE Journal of Oceanic Engineering*, pages 651–659.

[MacIver and Solberg, 2001] MacIver, M. and Solberg, J. (2001). Towards a biorobotic electrosensory system. *Autonomous robots*, 11:263–266.

[Maki et al., 2013] Maki, T., Shiroku, R., Sato, Y., Matsuda, T., Sakamaki, T., and Ura, T. (5-8 March 2013). Docking method for hovering type auvs by acoustic and visual positioning. *Underwater Technology Symposium (UT), 2013 IEEE International*, pages 1–6.

[Mintchev et al., 2012] Mintchev, S., Stefanini, C., Girin, A., Marrazza, S., Orofino, S., Lebastard, V., Manfredi, L., Dario, P., and Boyer, F. (14-18 May 2012). An underwater reconfigurable robot with bioinspired electric sense. *Robotics and Automation (ICRA), 2012 IEEE International Conference on*, pages 1149–1154.

[Moller, 1995] Moller, P. (1995). *Electric Fishes: History and Behavior*. Chapman & Hall.

[Morel et al., 2012] Morel, Y., Porez, M., and Ijspeert, A. (2012). Estimation of the relative position and coordination of mobile underwater robotic platforms through electric sensing. In *IEEE Conference on Robotics and Automation,*.

[Park et al., 2009a] Park, J.-Y., Jun, B.-H., Kim, K., Lee, P.-M., Oh, J.-H., and Lim, Y.-K. (2009.a). Improvement of vision guided underwater docking for small auv isimi. In *IEEE OCEANS 2009*.

[Park et al., 2009b] Park, J.-Y., Jun, B.-h., Lee, P.-m., and Oh, J. (2009b). Experiments on vision guided docking of an autonomous underwater vehicle using one camera. *Ocean Engineering*, 36(1):48–61.

[Rasnow, 1996] Rasnow, B. (1996). The effects of simple objects on the electric field of apteronotus. *Journal of Comparative Physiology A*, 3(178):397–411.

[Servagent et al., 2013] Servagent, N., Jawad, B., Bouvier, S., Boyer, F., Girin, A., Gomez, F., Lebastard, V., and Gossiaux, P.-B. (2013). Electrolocation sensors in conducting water bioinspired by electric fish. *IEEE Sensor Journal*, 13(5):1865–1882.

[Silverman et al., 2012] Silverman, Y., Snyder, J., Bai, Y., and MacIver, M. A. (2012). Location and orientation estimation with an electrosense robot. In *IEEE/RSJ Int. Conf. on Intelligent Robots and Systems*.

[Yuh et al., 2011] Yuh, J., Marani, G., and Blidberg, D. R. (2011). Applications of marine robotic vehicles. 4(4):221–231.